Article

Green Synthesis, Characterization, and Evaluation of Photocatalytic and Antibacterial Activities of Co_3O_4−ZnO Nanocomposites Using *Calpurnia aurea* Leaf Extract

Kemal Mohammed Gendo,* Raji Feyisa Bogale,* and Girmaye Kenasa
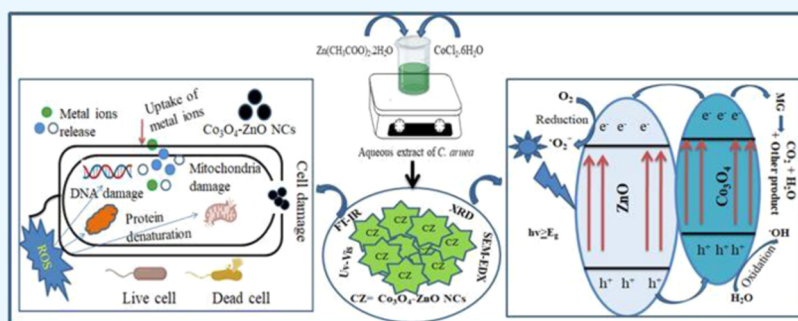
Read Online

ACCESS | Metrics & More | Article Recommendations | SI Supporting Information

ABSTRACT: The green synthesis of transition metal oxide nanocomposites using plant extracts is a new and effective method that avoids the involvement of hazardous chemicals. Nondegradable organic pollutants and antibiotic drug resistance have become serious public health issues worldwide. Hence, the main objective of this study is to synthesize Co_3O_4−ZnO nanocomposites using *Calpurnia aurea* leaf extract and evaluate its photocatalytic and antibacterial activities. The green synthesized particles were characterized using UV−vis spectra, Fourier transform infrared spectroscopy, X-ray diffraction techniques, and scanning electron microscopy combined with energy-dispersive X-ray studies. The synthesized particles were found to be crystalline in nature with average crystallite sizes of 23.82, 14.79, 15.99, 16.46, and 21.73 nm. Scanning electron microscopy shows the spherical morphology of Co_3O_4−ZnO NCs, and energy-dispersive X-ray analysis confirms the formation of highly pure ZnO NPs and Co_3O_4−ZnO NCs. The photocatalytic activity was performed under natural sunlight using malachite green as an organic dye pollutant. The green synthesized ZnO NPs, Co_3O_4 NPs, 1:4, 1:3, and 1:2 Co_3O_4−ZnO NCs showed high degradation efficiency after 60 min of irradiation. The synthetic material showed good potential against *Staphylococcus aureus* and *Escherichia coli*, with the highest growth inhibition recorded by 1:2 Co_3O_4−ZnO NCs. The kinetics study of the photocatalytic degradation was confirmed as pseudo first order, and the possible mechanisms for both photocatalytic and antibacterial activities were clearly determined.

1. INTRODUCTION

Water contamination poses a significant threat to our planet due to the growing human population and rapid technological advancements. Organic contaminants and bacteria are commonly encountered in the aquatic environment due to their high chemical stability and substrate nature.[1] A wide range of natural and synthetic dyes are used in the leather, textile, food, and plastic sectors. Among several dyes, malachite green (MG), a highly poisonous and carcinogenic dye, is widely used in industries but can cause carcinogenesis, chromosomal fractures, mutagenesis, teratogenicity, and pulmonary toxicity.[2,3] The chemical structure of the malachite green oxalate (MG) dye is shown in Figure 1. Despite antibiotic resistance, infectious diseases continue to rise, necessitating the development of novel technology to protect the environment from harmful chemicals and harmful microbes.[4]

Various approaches have been employed to remove MG dyes, including photocatalysis, biological treatment, ultrafiltration, and adsorption processes. Photodegradation is one of the most successful techniques because it decomposes harmful pollutants and converts them into harmless substances. As a result, heterogeneous photocatalysis is a promising area of study because it enables the complete mineralization of these environmentally harmful dyes.[3]

Metal and metal oxide nanoparticles have shown potential in photocatalysis and biomedicine. It is indicated that multi-
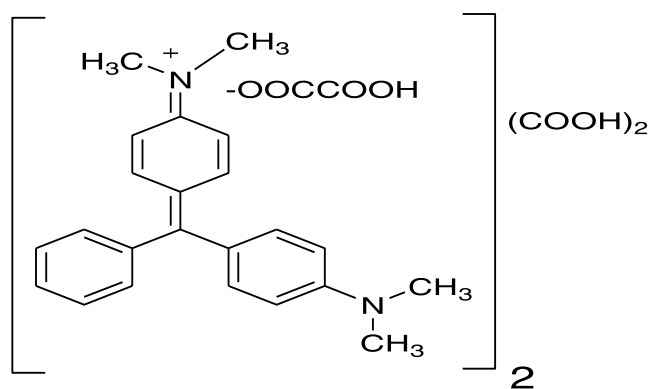
Figure 1. Chemical structure of malachite green oxalate (MG) dye.

metallic oxide nanoparticles exhibit better beneficial properties than single metallic oxide nanoparticles.[5] Among metal oxides, zinc oxide (ZnO), an intriguing n-type direct band gap semiconductor, has drawn attention owing to its appealing properties of green characteristics, excellent stability, single-step synthesis route, and low price.[6] Meanwhile, cobalt oxide (Co_3O_4) has dual attractive properties due to its magnetic and semiconducting properties.[7] Co_3O_4 is a low-band gap energy (Eg) semiconductor, unveiling substantial photocatalytic properties.[8] Co_3O_4 addition to wide Eg semiconductors enhances the cocatalyst sustenance and stability. This can alter nanocomposites' electrical and physicochemical properties, enabling new applications like water treatment. Metal oxide-based nanocomposites are promising for photocatalysis and biomedicine.[9] Metal oxide-based nanocomposites, particularly transitional ones, are promising for photocatalysis and biomedicine due to their nontoxic nature, large surface area, and high biological activity.[10,11]

Nanocomposites can be produced by different techniques, such as chemical, physical, and green methods.[12,13] Among these, green synthesis is a sustainable, eco-friendly method for synthesizing various nanomaterials, including metal oxides, hybrid materials, and bioinspired materials. It is a novel development that has gained significant attention as a feasible alternative to traditional chemical and physical processes. It reduces the destructive effects of traditional methods and uses plants, fungi, bacteria, and algae as reducing agents and capping agents. These biological materials help control morphology and stabilize nanoparticles, reducing the use of toxic chemicals and extreme environments.[4,14]

The synthesis process of green nanoparticles involves three phases: activation, growth, and termination. During the activation phase, plant metabolites aid in recovering metal ions from salt precursors, while biomolecules act as green reducing agents. The growth phase involves more biological reduction of metal atoms. Although prolonged nucleation may cause synthesized NPs with deformed morphologies to aggregate, the growth stage improves the thermodynamic stability of the NPs. The termination phase is the last stage of green NP synthesis, during which plant metabolites seal off NPs when they finally achieve their most actively favorable and stable shapes. The reduction of metal ion oxidation states, which results in a color shift that serves as the initial sign of qualitative nanoparticle production, is described in these steps.[15,16]

Calpurnia aurea, (*C. aurea*), a plant of the *Fabaceae* family, is a small, multistemmed tree in Sub-Saharan Africa and India, that is used in traditional medicine for treating various ailments and parasitic infestations. *C. aurea* (Ait.) Benth has several local names in Ethiopia, including digita in Amharic and chekka in Afaan Oromo. Its high content of tannins, flavonoids, terpenoids, saponins, steroids, glycosides, and alkaloids aids in metal ion reduction and chelating agents.[4] Secondary metabolic compounds from this plant have antibacterial capabilities against pathogenic bacterial strains like *E. coli*, *S. aureus*, and others.[17] Therefore, *C. aurea* is chosen as the raw material for the green synthesis of Co_3O_4–ZnO nanocomposites in the current study due to its phytochemical constituents and biological activities. Figure 2 is a schematic illustrating a green synthesis mechanism of Co_3O_4–ZnO nanocomposites using *C. aurea* leaf extracts.

Numerous studies have explored the synthesis and application of n-type ZnO-based semiconductor materials in combination with other materials. For instance, Puttarajuet al.[18] developed ZnO/NiO nanocomposites using *Phyllanthus-niruri L.* extract for photocatalytic and biological activities. Bordbar et al.[19] reported the green synthesis of CuO/ZnO nanocomposite using *Melissa Officinalis L.* leaf extract for photocatalytic degradation. Kalaivani& Ravi,[20] reported the green synthesis of CdO-ZnO NCs using water hyacinth (*Eichhornia crassipes*) for nanofertilizer application. Aragaw et al.,[21] synthesized a p-Co_3O_4/n-ZnO composite for photo-
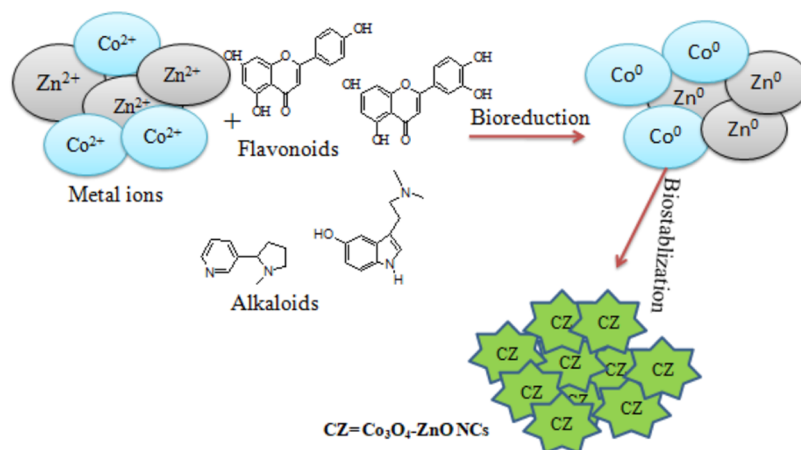
Figure 2. Schematic representation for the *C.aurea*-mediated green synthesis of Co_3O_4–ZnO nanocomposites.

catalytic applications. However, improved catalytic efficiencies and antibacterial activity still need further exploration of green synthesis ZnO-based nanocomposites.

On the other hand, there is no reported study on the green synthesis of Co_3O_4–ZnO nanocomposites using *C. aurea* leaf extract. Thus, in view of this respect, the current work is focused on the green synthesis of Co_3O_4–ZnO NCs using *C. aurea* leaf extract for photocatalytic and antibacterial activities. The study also investigates the impact of reaction parameters on the synthesis and photocatalytic activity of these nanocomposites. The Co_3O_4–ZnO NC was analyzed comprehensively by several methods, including UV–vis, FT-IR, XRD, and SEM-EDX.

2. MATERIALS AND METHODS

2.1. Chemicals and Reagents. Zinc acetate dihexahydrate ($Zn(CH_3COO)_2 \cdot 2H_2O$, 98%), cobalt chloride hexahydrate ($CoCl_2 \cdot 6H_2O$, 98%), sodium hydroxide (NaOH, 99.8%), ferric chloride ($FeCl_3$, 99% from LobaChemie, India), hydrochloric acid (HCl, 37% India), sulfuric acid (H_2SO_4, 98%), nitric acid (HNO_3, 65%), acetic anhydride (($CH_3CO)_2O$, 99.5%), dimethyl sulfoxide (($CH_3)_2SO$, 99%) acetic acid (CH_3COOH, 99.5%), potassium iodide (KI, 98.5%), iodine (I_2, 99%), ethanol (CH_3CH_2OH, 98%), Muller Hinton Agar (MHA, Merck chemical company), and malachite green oxalate ($C_{52}H_{54}N_4O_{12}$, 99.5%) were used. All chemicals and reagents were of analytical grade and were used exactly as received, with no further purifications.

2.2. Preparation of *C. aurea* Leaf Extract. *2.2.1. Plant Material Collection and Preparation.* A fresh leaf of *C. aurea* was collected from the University of Wollega's Botanical Garden in Ethiopia in November 2022. Its scientific name was identified and authenticated by the Wollega University Department of Biology. The preparation of *C. aurea* aqueous leaf extract was done following the procedure reported in ref 22.[22] The leaf samples were washed with tap water and deionized water and dried completely at room temperature for 15 days under shade to remove the moisture content. The dry materials were crushed into a fine powder using an electrical miller. The extraction process was performed by taking 10 g of leaf powder in a 250 mL beaker and then adding 100 mL of distilled water. To avoid light exposure, the resulting portions have been covered in aluminum foil and boiled for about 20 min at 60 °C. After cooling to room temperature, the suspension was filtered through Whatman filter paper No. 1. Finally, the filtrate was placed in a glass bottle covered in aluminum foil and refrigerated at 4 °C for future use.[22] Figure S1 depicts the schematic techniques for preparing *C. aurea* leaf extract.

2.2.2. Qualitative Phytochemical Analysis. Phytochemicals, non-nutritive plant substances with anti-inflammatory and disease-fighting properties, were identified in *C. aurea* leaf extract through secondary metabolite qualitative analysis.[23] The *C. aurea* leaf extract was tested for alkaloids, flavonoids, tannins, saponins, terpenoids, and steroids. A reddish-brown precipitate was found in Wagner's test, while a yellow-colored precipitate was found in the lead acetate test. Tannins and phenolic compounds were detected through the ferric chloride test, while saponins were detected through the foaming test. Terpenoids were detected through the Liebermann test, and steroids were detected through the Liberman*n*-Burchards test.

2.3. Optimization of Parameters. *2.3.1. Optimization of Some Parameters for Synthesis of C. aurea Leaf Extract-Mediated Co_3O_4, ZnO, NPs, and Co_3O_4–ZnO NCs.* The quality, stabilization, quantity, and yield rate of nanoparticles are influenced by various parameters such as pH, temperature, metallic salt concentration, and phytochemical profile of plant leaf particles.[24] These characteristics are crucial for understanding the impact of environmental features on nanoparticle synthesis. The study investigated the optimal method for synthesizing ZnO, Co_3O_4NPs, and Co_3O_4–ZnO NCs by varying the reaction parameters. The UV–visible spectrum was used to verify particle production, determining the best reaction conditions for nanoparticles and nanocomposites.

2.3.1.1. Effect of pH. Numerous extractions from plants had different pH values, which necessitated further modifications prior to the biosynthesis of the NPs and NCs. Furthermore, it has been found that the pH influences the activity of functional groups in plant extracts. In this study, the pH of the solution was varied from 5 to 12 for ZnO NPs and Co_3O_4–ZnO NCs, and from 5 to 13 for Co_3O_4 NPs by adding a dropwise NaOH solution (2 M).

2.3.1.2. Effect of Volume of Calpurnia aurea Leaf Extract. The synthesis of NPs and NCs from plant extracts is greatly affected by the kinds of biomolecules present in plant extracts along with the volume utilized.[25] In the current study, 100 mL of 0.1 M precursor salt solution was mixed with 10, 20, 30, 40, and 50 mL of *C. aurea* leaf extract.

2.3.1.3. Effect of Concentration of Metal Salt Precursors. Accordingly, before synthesizing Co_3O_4, ZnO NPs, and Co_3O_4–ZnO NCs, 100 mL of metal precursor (Zn-($CH_3COO)_2.2H_2O$ and $CoCl_2.6H_2O$ as zinc and cobalt precursors, respectively) with varied concentrations (0.05, 0.1, 0.2, and 0.5 M) were used to evaluate the influence of metal precursor. The mole ratios of cobalt to zinc precursors in the synthesis of Co_3O_4–ZnO NCs also had an effect on the absorption peak of Co_3O_4–ZnO NCs. Thus, the effect of cobalt and zinc precursor ratios on the synthesis of Co_3O_4–ZnO NCs was also investigated using several mole ratios (1:1, 1:2, 1:3, 1:4, 2:1, and 3:1) to determine the optimal reaction ratio.[26]

2.3.1.4. Effect of Reaction Temperature. To study the effect of temperature on the formation of ZnO, Co_3O_4 NPs, and Co_3O_4–ZnO NCs, different temperatures (room temperature, 50, 70, 80, and 90 °C) were used to obtain the optimum temperature for the synthesis of these nanomaterials.

2.3.2. Optimization of Some Experimental Conditions for the Photocatalytic Activities of Green Synthesized Co_3O_4–ZnO NCs. Optimization is important to maximize the degradation rate of the MG dyes. Several parameters had a significant impact on the dye-degrading ability of the synthesized Co_3O_4–ZnO NCs and were optimized. Optimization was performed for the effects of pH, initial dye concentration, catalyst loading, and irradiation time.[27,28]

2.4. Synthesis of *C. aurea* Leaf Extract-Mediated Co_3O_4, ZnO, NPs, and Co_3O_4–ZnO NCs. *2.4.1. Green Synthesis of ZnO NPs.* The synthesis of ZnO nanoparticles was carried out using the method of Elumalai and Velmurugan,[29] with slight modifications. Accordingly, 100 mL of a 0.1 M Zn ($CH_3COO)_2 \cdot 2H_2O$ solution was taken, and 30 mL of *C. aurea* leaf extract was added and mixed in a 250 mL flask. Then, 2.0 M NaOH was added dropwise until the pH reached 11, and the mixture was stirred for 2 h under constant conditions at 60 °C. The precipitate produced by zinc ion reduction was centrifuged at 10,000 rpm for 10 min. The resultant precipitate was washed repeatedly with distilled

water, followed by absolute ethanol, dried in an oven at 60 °C for 6 h, and then calcinated in a muffle furnace for 2 h at 500 °C.

2.4.2. Green Synthesis of Co$_3$O$_4$ NPs. The synthesis took place according to Haq et al.[30] with some modifications. In a conical flask, 100 mL of 0.1 M CoCl$_2$.6H$_2$O and 30 mL of *C. aurea* leaf extract were added to produce the formulated Co$_3$O$_4$ NPs. The pH was then kept at 13 by adding a 2 M solution of NaOH dropwise while continuously stirring. The flask was then placed on a hot plate with a magnetic stirrer and heated at 60 °C for 2 h. After cooling at room temperature, the solution was centrifuged (10,000 rpm for 10 min) to obtain the pellet, which was then washed many times with distilled water and ethanol to eliminate contaminants. The Co$_3$O$_4$ NPs were dried in an oven at 60 °C for 6 h before being calcinated in a muffle furnace for 2 h at 500 °C.

2.4.3. Green Synthesis of Co$_3$O$_4$–ZnO NCs. C.aurea leaf-mediated Co$_3$O$_4$–ZnO nanocomposites were successfully synthesized using optimum reaction parameters. In the preparation of 1:1 mol ratio Co$_3$O$_4$–ZnO nanocomposites, a 0.1 M precursor solution with a Co:Zn mole ratio of 1:1 was prepared by weighing 2.379 g of the CoCl$_2$.6H$_2$O and 2.195 g of the Zn (CH$_3$CO$_2$)$_2$·2H$_2$O and dissolving them together in 100 mL of deionized water, followed by the addition of 30 mL of the *C. aurea* leaf extracts. This was followed by adjustment of the pH of the solution to 11 by dropwise addition of an aqueous solution of NaOH (2 M). The solution was magnetically stirred at 60 °C for 2 h. The precipitate was separated from the reaction suspension by centrifugation at 10,000 rpm for 10 min. The obtained precipitate was washed with deionized water and ethanol repeatedly. Subsequently, it was dried in an oven at 60 °C for 6 h before being calcinated at 500 °C for 2 h to produce quite crystalline pure-phase nanocomposites. For the synthesis of 1:2, 1:3, 1:4, 2:1, and 3:1 mol ratio compositions of Co$_3$O$_4$-ZnO, the same technique was followed as for the synthesis of the 1:1 mol ratio.

2.5. Characterization of Green Synthesized Co$_3$O$_4$, ZnO NPs, and Co$_3$O$_4$–ZnO NCs. A UV–vis study was conducted to evaluate the visual properties of Co$_3$O$_4$, ZnO NPs, and Co$_3$O$_4$–ZnO NCs.[31] The absorbance was recorded in a quartz cell at room temperature, and the band gap energy was calculated using the Tauc/David-Matt model.[32] The band gap energy (E_g) of Co$_3$O$_4$, ZnO NPs, and Co$_3$O$_4$–ZnO NCs was calculated from the Tauc plot by using the Tauc/David-Matt model (eq 1).

$$Ah\nu = \alpha(h\nu - E_g)^{n/2} \tag{1}$$

where *A*, *h*, *v*, *α*, and E_g are constant, Planck's constant, light frequency, absorption coefficient, and energy band gap, respectively.

Fourier transform infrared spectra were used to examine different functional groups in the 4000−400 cm^{-1} region. The KBr pellet approach was used to identify the most likely biomolecule and nanoparticle production using *C. aurea* leaf extract.[23] X-ray diffraction was conducted to study the phase formation, size, purity, and crystallinity of the synthesized nanoparticles and nanocomposites. The diffraction patterns were recorded from 10 to 80 with 2θ angles using Cu−K$_\alpha$ (λ = 1.54 Å) radiation operated with accelerating voltage and applied current of 40 kV and 30 mA, respectively, and the average crystallite size was calculated using the Debye−Scherrer equation (eq 2).[33]

$$D = 0.94\lambda/\beta \cos\theta \tag{2}$$

where *D* is the crystallite size, λ is the X-ray source wavelength, β is the full width at half-maximum (fwhm) of a peak, and θ is the Bragg diffraction angle.

Scanning electron microscopy (SEM) was used to examine nanoscale materials, providing better information about the sample due to its significant depth of focus. SEM images can be used to collect nanoparticle length and width data and obtain the average size using image visualization software.[34]

2.6. Photocatalytic Degradation of Malachite Green Dye and Recyclability of Photocatalyst. The photocatalytic efficacy of Co$_3$O$_4$−ZnO NCs was tested under sunlight as a source of visible light and MG dye as a model pollutant under optimum reaction conditions. The photocatalytic performance of samples was done by adding 50 mg of photocatalyst (Co$_3$O$_4$, ZnO NPs, or Co$_3$O$_4$−ZnO NCs) to 100 mL of 10 ppm of MG solution. The suspension was stirred in the dark for 30 min before exposure to visible light to improve the adsorption−desorption equilibrium. Before exposing the suspension to visible light (*t* = 0), an initial sampling was performed. The suspension was then irradiated under sunlight and stirred for 60 min. An aliquot of the sample was taken out after each 10 min, and the photocatalyst was removed by centrifuging the solution. These aliquots of the sample were then evaluated using a UV−visible double-beam spectrophotometer to look for alterations in intensity associated with the MG max, which shows at 618 nm.[35] The photocatalyst activity for photocatalytic degradation of MG dye (*D*%) was estimated employing the following formula: (eq 3), where the amount of MG is directly proportional to the intensity of the absorption peak at 618 nm. After complete decolorization, the catalyst was centrifuged, treated with distilled water and ethanol several times, and subsequently dried at room temperature before utilization. Using the same procedure, photocatalytic degradation was performed for three cycles under visible light, and the percent degradation for each experiment was calculated.

$$D\% = \left(\frac{A_o - A_t}{A_o}\right) \times 100 \tag{3}$$

where A_o is the absorbance at the initial time and A_t is the absorbance at a time after degradation at λ_{max} of MG.

2.7. Antibacterial Activity of Green Synthesized Co$_3$O$_4$, ZnO NPs and Co$_3$O$_4$−ZnO NCs. The antibacterial properties of Co$_3$O$_4$, ZnO NPs, and Co$_3$O$_4$−ZnO NC were tested on Muller Hinton Agar (MHA) by using the disk diffusion method. The antibacterial activities of nanomaterials produced from *C. aurea* leaf extract were tested by using two different bacterium varieties: *Staphylococcus aureus* ATCC 25926 and *Escherichia coli* ATCC 25922. About 100 μL (1.5 108 CFU mL^{-1}) of each bacterium's active culture (grown on Muller Hinton broth medium for 24 h at 37 °C) was stained evenly on Muller Hinton medium in Petri plates by a sterile glass spreader, cooled in a water bath, and vigorously mixed by flask swirling. Wells were made in each agar culture medium using a sterile cork borer (6 mm in diameter), and dry 6 mm sterile paper disks soaked with test samples (concentration 100−12.5 mgmL^{-1}) were set on Muller Hinton plates evenly implanted with test bacterial inoculums. A disk impregnated with erythromycin (15 g/disk) and DMSO was employed as a positive and negative control, respectively, to test the effect of the standard and solvent on the pathogens, respectively. The

inoculated Petri plates were stored in an incubator (at 37 °C) for 24 h, and the hindered bacterial growth was visible as clear zones surrounding the disk. The diameter of the zone of inhibition was then used to calculate the antibacterial activity.[36]

2.8. Statistical Analysis. All data obtained from UV−vis, XRD, FT-IR, and SEM characterization of synthesized nanoparticles and nanocomposite was analyzed using Origin-8 software, and IBM SPSS Software was used to interpret the antibacterial activities of synthesized nanomaterials.

3. RESULT AND DISCUSSION

3.1. Phytochemical Analysis of *C. aurea* Aqueous Leaf Extract. The phytochemical analysis was carried out to justify the various types of bioactive components found in *C. aurea* leaf extract by employing a different type of chemical, as illustrated in Figure S2. The phytochemical study of the *C. aurea* plant's aqueous extract confirmed the existence of phytoconstituents that needed to be identified. Table 1 shows

Table 1. Lists of Phytochemical Screening of the *C. aurea* Leaf Extracts[a]

s/no.	secondary metabolites	tests	observations	results
1	alkaloids	Wagner's test	reddish-brown precipitate	++
2	flavonoids	lead acetate test	formation of yellow color which disappears on the addition of dilute HCl	++
3	phenols	ferric chloride test	formation of dark green solution	+
4	saponins	frothing (foam) test	formation stable froth that persists for at least 2 min	+
5	steroids	Libermann−Burchards test	formation of dark green color	+
6	tannins	ferric chloride test	blue-black color	+
7	terpenoids	Liebermann test	formation of yellow color	−

[a]"+", "−" sign indicates the presence and absence of phytoconstituents, respectively, whereas ++ indicates the most phytoconstituents found in the *C.aurea* leaf extract.

that the *C. aurea* leaf extracts were high in phytochemical elements, such as phenols, saponins, flavonoids, tannins, and alkaloids, among others. The FT-IR results also revealed that the bioactive substances comprise the O−H, C−O, C−H, and C=O functional groups and operate as reducing, capping, and stabilizing agents in the formation of nanoparticles and nanocomposites.

3.2. Effects of Reaction Parameters on the Synthesis of Co_3O_4, ZnO NPs and Co_3O_4−ZnO NCs. In this study, the pH of the solution was varied from 5 to 12 for ZnO NPs and Co_3O_4−ZnO NCs, whereas it was vaired from 5 to 13 for Co_3O_4 NP synthesis to get optimum pH. For the acidic solution (pH = 5), no surface plasmon resonance (SPR) band of nanoparticles developed. However, changing the pH to alkaline resulted in the appearance of the SPR band at distinct wavelengths. The intensity of UV−vis absorption increased as the pH of the reaction solution increased, owing to the increased concentration of the produced nanoparticles and nanocomposites. This occurrence can be explained by the fact that high pH values enhance the creation of nucleation centers and increase the reduction of zinc and cobalt into the

corresponding metal oxide NPs, resulting in the synthesis of a large amount of NPs. A high-intensity peak was found in SPR at pH 11, 13, and 11 for ZnO, Co_3O_4 NPs, and Co_3O_4−ZnO NCs, respectively. As a result of the acquired data, these pH values were optimized due to a better peak and maximum absorption peak intensity, and the rest of the studies were performed at these pHs.

In a similar manner, different volumes of *C. aurea* leaf extract were used, and the results showed that as the volume of the extracted plant increased from 10 to 50 mL, the absorption peaks decreased, with 30 mL of *C. aurea* leaf extract exhibiting the highest absorption. The concentration was increased to 30 mL because a strong peak with high intensity was observed. This shows that the presence of 30 mL of bioactive chemicals was sufficient to reduce metal ions in the reaction mixture and cap the nanoparticle surfaces by preventing their aggregation.[37]

100 mL of metal precursor with varied concentrations (0.05, 0.1, 0.2, and 0.5 M) were used to evaluate the influence of metal precursor concentration. The intensity of the absorption peak increased as the concentration of the metal salt solution increased from 0.05 to 0.1 M. The intensity of the absorption peak decreased as the concentration was increased to 0.2 and 0.5 M. As a result, it was found that raising the concentration of metal ions beyond the optimal value resulted in a decrease in nanoparticle formation. This is most likely because greater concentrations of Zn $(CH_3COO)_2.2H_2O$ and $CoCl_2.6H_2O$ cause agglomeration of ZnO and Co_3O_4 particles rather than the development of capped nanoparticles in a colloidal solution.[38] Then, 0.1 M was chosen as the optimum concentration for the synthesis of ZnO and Co_3O_4 NPs because it produced a sharp peak indicating the formation of nanoparticles.[25] Finally, several mole ratios of cobalt to zinc precursors (1:1, 1:2, 1:3, 1:4, 2:1, and 3:1) were utilized to determine the optimal reaction ratio, and 1:4, 1:3, and 1:2 were optimized because they provided the highest UV−vis absorbance value at the longest wavelength (red shift), which indicates high yield and stability.

Various temperatures (room temperature, 50, 70, 80, and 90 °C) were used to obtain the optimum temperature for synthesis; 60 °C was optimized for all ZnO NPs, Co_3O_4, and Co_3O_4−ZnO NCs. This result could be explained by the rapid reduction of metal ions at this temperature. However, increasing the temperature above the optimal range resulted in a decrease in the intensity of the absorption peak. This observation may further suggest that the simultaneous aggregation of NPs and NCs happened as a result of the heat-induced breakdown of the reducing and capping agents present in plant extracts.[39] Green techniques were used for the synthesis of Co_3O_4, ZnO NPs, and Co_3O_4−ZnO NCs after each parameter was optimized.[26] The results of optimization for the synthesis parameters of ZnO, Co_3O_4 NPs, and Co_3O_4−ZnO NCs are indicated in Figures S3, S4, and S5, respectively.

3.3. Green Synthesis of ZnO, Co_3O_4 Nanoparticles and Co_3O_4−ZnO Nanocomposites. *C. aurea* leaf extract was high in phytochemical compounds such as phenols, saponins, flavonoids, tannins, and alkaloids, which help in the synthesis of ZnO, Co_3O_4 NPs, and Co_3O_4−ZnO NCs. During the synthesis of NCs, these phytochemicals work as reducing agents, converting metal ions into the appropriate nanoparticles, and stabilizing agents, preventing NC aggregation.[40] During the synthesis of ZnO NPs, a yellowish-white precipitate was formed after the addition of the greenish *C. aurea* leaf extract to the colorless zinc acetate dihydrate solution,

indicating the formation of ZnO NPs. During the synthesis of Co_3O_4 NPs, adding the greenish C. aurea leaf extract to the pale pink cobalt chloride hexahydrate changes the solution to dark brown first and subsequently to black, indicating the development of Co_3O_4 NPs. Co_3O_4–ZnO *nanocomposites* have been successfully synthesized in an eco-friendly manner using *C. aurea* leaf extract as a stabilizing and reducing agent. During the synthesis of Co_3O_4–ZnO NCs, upon addition of greenish *C. aurea* leaf extract to the pink color of precursor mixtures, the final mixture was turned to a dark green color and then a dark brown precipitate. A summary of schematic representations of the green synthesis of ZnO NPs, Co_3O_4 NPs, and Co_3O_4–ZnO NCs is shown in Figure S6, which is given in the Supporting Information.

3.4. UV–Vis Absorption Spectral Analysis.
The UV–visible spectra of *C. aurea* leaf extract (Figure 3) exhibit an
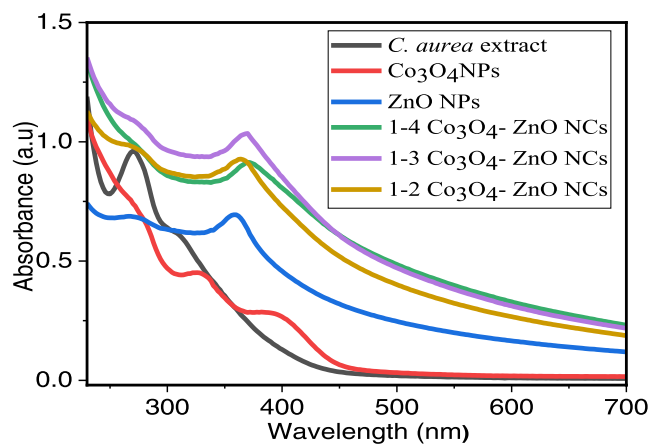

Figure 3. UV−vis spectrum of green synthesized ZnO NPs, Co_3O_4 NPs, Co_3O_4–ZnO NCs, and *C.aurea* leaf extract.

absorption band at 270 nm caused by $\pi \rightarrow \pi*$ transitions, indicating the presence of phenolic chemicals involved in the green production of NPs and NCs. On the other hand, the UV−vis spectrum reveals a characteristic absorption peak of green synthesized Co_3O_4 at 326 and 392 nm, ZnO NPs at 358 nm, 1:2 Co_3O_4−ZnO at 370 nm, 1:3 Co_3O_4−ZnO at 368 nm, and 1:4 Co_3O_4−ZnO NCs at 364 nm, as shown in Figure 3. The intrinsic band gap absorption of ZnO due to electron transitions from the valence band to the conduction band can be assigned to the characteristic absorption peak of ZnO at 358 nm. The observed results were completely in line with Ramesh et al.[41] who showed the efficacy of *Solanumnigrum* leaf in the production of ZnO-NPs with intense SPR at 358 nm. When compared to the wavelength of bulk ZnO, which appeared at 385 nm, the adsorption edges of the ZnO NPs were efficiently blue-shifted.[42] This shift in the absorbance peak was associated with a decrease in particle sizes for ZnO NPs generated in the presence of *C. aurea* leaf extract, which is attributed to the quantum confinement effect.[29]

The UV−vis spectroscopy results revealed that the typical peaks of Co_3O_4 NPs were found at 326 and 392 nm, which were in the maximum wavelength ranges of 200−350 nm and 380−600 nm, respectively. These peaks are attributed to $O^{2-} \rightarrow Co^{2+}$ and $O^{2-} \rightarrow Co^{3+}$ charge transfer processes, respectively.[43] When compared to pure ZnO NPs, the Co_3O_4−ZnO NCs showed a significant red shift in absorbance and strong visible light absorbance, confirming the presence of

visible light responsive Co_3O_4 NPs in the nanocomposites and hinting at band gap narrowing.[44] The optical absorbance of semiconductor NCs is also affected by parameters such as oxygen deprivation, grain defects, nanoparticle structure, and size.[45]

The Tauc equation was used to determine the band gap energy of the synthesized material.[46] The band gap energies of Co_3O_4, ZnO NPs, and Co_3O_4−ZnO NCs were determined by plotting $(h\nu)^2$ vs hv, and the Tauc plots produced are shown in Figure 4. The band gap energy was calculated to be 2.62 eV for
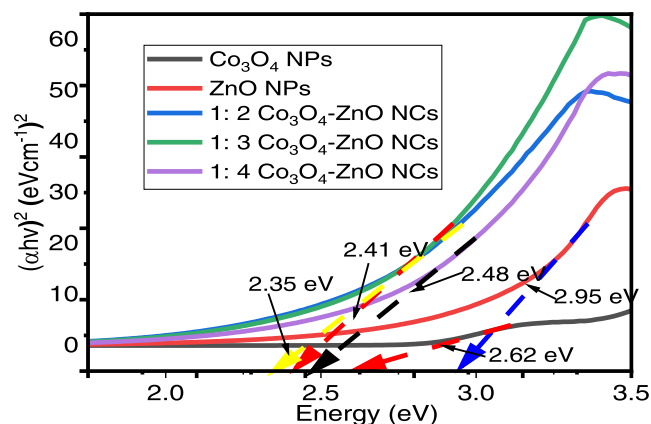

Figure 4. Band gap energy for Co_3O_4, ZnO NPs, and Co_3O_4−ZnO NCs.

Co_3O_4, which is slightly related to the reported values of (2.46 eV),[47] (2.85 eV),[48] 2.92 eV for ZnO NPs, which are similar to (2.92 eV),[49] 2.35 eV for 1:2 Co_3O_4_ZnO, 2.41 eV for 1:3 Co_3O_4 − ZnO and 2.48 eV for 1:4 Co_3O_4_ZnO NCs, as shown in the Tauc plot (Figure 4). The pure ZnO NPs disclosed an optical band gap energy of 2.96 eV, which was decreased for Co_3O_4−ZnO NCs with increasing cobalt ion concentrations with various mole ratios. The incorporation of visible light absorptive Co_3O_4 in the Co_3O_4−ZnO NCs accounts for the considerable red shift (2.48, 2.41, and 2.35 eV) in the band gap energy of the Co_3O_4−ZnO NCs over the pure ZnO NPs. Compared with bare ZnO NPs, the inclusion of Co_3O_4 NPs improved band gap absorption. The band gap for ZnO-NPs is relatively large, confirming that increasing the Co_3O_4 ratio in the nanocomposites resulted in a noticeable decrease in the band gap.[50]

3.5. Fourier Transformed Infrared (FT-IR) Spectroscopy Analysis.
The Fourier transform infrared spectra were analyzed using the FT-IR (PerkinElmer, 65) model in the range of 4000−400 cm^{-1}, to identify possible biomolecules as well as nanoparticle formation, which may be responsible for capping and efficient stabilization to prevent the overall growth of nanoparticles and nanocomposites using *C. aurea* leaf extract.[51] Figure 5 displays the FT-IR spectra of *C. aurea* leaf extract under the wavenumber range of 4000−400 cm^{-1}. FT-IR spectra also reveal various peaks at 962, 1271, 1607, 1732, 2337, 2925, and 3366 cm^{-1}, due to C−H out-of-plane bending and C−O stretching, corresponding to N−H stretching of the functional group of ammines, C=O stretching, C−H stretching, and O−H stretching functional groups, respectively. The presence of these groups illustrates that *C. aurea* can be utilized in the synthesis of Co_3O_4−ZnO nanocomposites. The emergence of the O−H peak indicates the existence of phenolic chemicals, which may be responsible for the
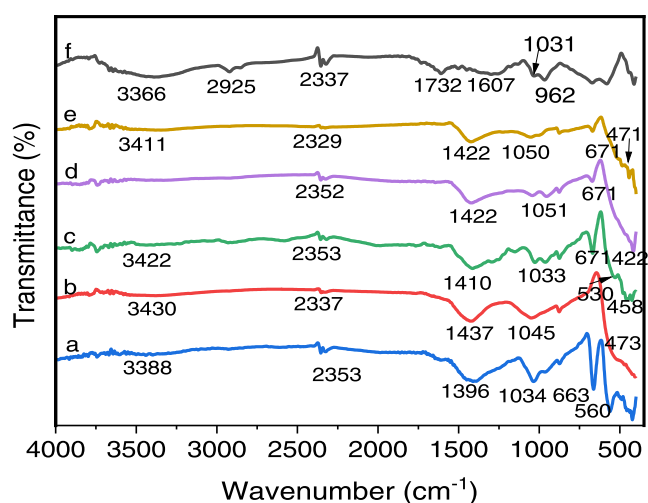
Figure 5. FT-IR spectrum of green synthesized (a) Co_3O_4, (b) ZnO NPs, (c) 1:2 Co_3O_4–ZnO NCs, (d) 1:3 Co_3O_4–ZnO NCs, (e) 1:4 Co_3O_4–ZnO NCs, and (f) *C. aurea* leaf extract

demonstrates that Co_3O_4–ZnO composites were successfully produced.

Despite frequent washing, the analysis shows that the presence of carbonyl, amine, and phenolic chemicals bound to the surface of the produced material improves stability by covering the metallic nanoparticles. In the absence of other strong ligating agents in adequate concentration, secondary metabolites such as flavonoids or terpenoids conjugated with nanoparticles adsorb on the nanoparticles surface via contact through carbonyl groups or electrons.[56] Overall, the FT-IR confirms the presence of different phytochemical compounds such as phenolic groups, flavonoids, and carbonyl groups in *C. aurea* leaf extract, which are used as reducing, capping, and stabilizing agents in the green synthesis of Co_3O_4, ZnO NPs, and Co_3O_4–ZnO NCs.

3.6. X-ray Diffraction (XRD) Analysis. The X-ray diffraction (XRD) method is suggested for determining the crystallinity of the nanomaterials. Synthesized materials (ZnO, Co_3O_4 NPs, and their composites with varying mole ratios) were subjected to intense rays from an XRD machine, which penetrated through them to offer important data regarding their crystallinity and average particle size structure.[57] Figure 6

Figure 6. XRD spectrum of green synthesized (a) ZnO NPs, (b) Co_3O_4 NPs, (c) 1:2 Co_3O_4–ZnO NCs, (d) 1:3 Co_3O_4–ZnO NCs, and (e) 1:4 Co_3O_4–ZnO NCs using *C. aurea* leaf extract

nanoparticle stabilization process. The presence of C=O could indicate the presence of aldehydes, esters, flavonoids, or ketones.[52]

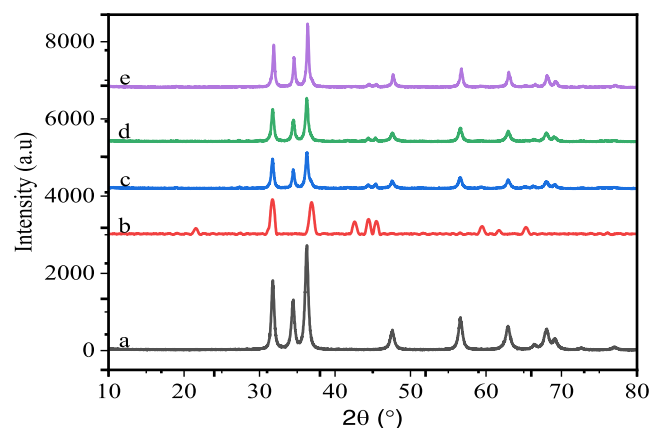Figure 5 shows the FT-IR spectra of synthesized Co_3O_4, ZnO NPs, and Co_3O_4–ZnO NCs. Absorption bands for Co_3O_4 NPs at 1034, 1396, 2353, and 3388 cm^{-1} may have been attributed to the C—O group of primary alcohol, —C-H stretching, C=O vibration, and — O—H stretching, respectively, which is found to be in good agreement with the literature report before.[43] Other strong absorption bands also appeared at 560 and 658 cm^{-1} in the FT-IR spectra of Co_3O_4 NPs and may be assigned to the stretching vibration mode of Co—O, which corresponds to the tetrahedral and octahedral coordination of Co^{2+} and Co^{3+}, respectively. Based on the previous research by Yulizar al.,[53] this result indicates that Co_3O_4 has been formed.

ZnO NPs FT-IR absorption bands were found at 473, 870, 1045, 1437, 2350, and 3373 cm^{-1}. The weak broad bands at 3373 and 2350 cm^{-1} were attributed to O—H stretching of flavonoids, polyphenols, and C=O groups on the surface of ZnO crystal nanostructures that may be present in *C. aurea* leaf extract, indicating that the bending frequencies of H_2O reveal the water content on the surface of nanoparticles. Furthermore, the 473 cm^{-1} peak reflects the stretching vibrations of zinc and oxygen bonds, indicating the production of ZnO nanoparticles. Consistent with our findings, FT-IR analysis of green-produced ZnO-NPs revealed that the Zn—O absorption band at 485,[54] 400, and 600 cm^{-1} is ascribed to Zn—O.[55] Weak peaks of absorption of C=O bonds around 2353, 2337, 2353, 2352, and 2329 cm^{-1} in synthesized materials indicate the formation of CO_2 molecules, which may absorb during synthesis.[56] The absorption peaks appearing at 1034, 1045, 1033, 1051, and 1050 cm^{-1} in the FT-IR spectra of Co_3O_4, ZnO NPs at 1:2, 1:3, and 1:4 can be assigned to C—O stretching, which might be due to primary alcohol. Various peaks were observed at 419, 441, 458, and 473 cm^{-1} in the FT-IR spectra of synthesized materials, which corresponded to stretching vibrational modes of Zn—O, whereas the peak at 671 cm^{-1} corresponded to stretching vibrational modes of Co—O in Co_3O_4–ZnO NCs FT-IR analysis. Therefore, the existence of Co—O and Zn—O

exhibits XRD patterns of ZnO, Co_3O_4, and Co_3O_4–ZnO samples. As shown in this figure, the XRD patterns of the ZnO sample at the 2θ values of 31.76, 34.44, 36.24, 47.57, 56.61, 62.90, 66.59, 68.00, 69.10, 72.62, and 77.01° were indexed as (100), (002), (101), (102), (110), (103), (200), (112), (201), (004), and (202) planes, respectively, which are in good agreement with those of powder ZnO obtained from the International Center of ZnO.[58]

Similarly, from the powdered XRD study of Co_3O_4 NPs, the diffraction peaks appeared at 2θ values of 21.56, 31.72, 36.90, 44.44, 45.48, 59.47, and 65.29°, which were indexed as (111), (220), (311), (400), (222), (511), and (440), respectively, and the synthesized material was confirmed to be Co_3O_4 NPs,[48] and JCPDS-042−1467. These diffraction peaks could be indexed as the face-centered cubic phase of the Co_3O_4 material.[59] However, the unidentified peaks observed in the XRD of Co_3O_4 might be due to the presence of some organic compounds originating from the aqueous extract of *C. aurea* leaf extract.[48,60] Moreover, the diffraction peaks appearing at 2θ values of 34.58, 44.51, 45.38, 47.70, 56.73, 63.05, 66.51, 68.12, 69.21, and 77.12° were indexed as (002), respectively, in

all ratios of Co_3O_4–ZnO NCs, which confirm the well-known combination of Co_3O_4 and ZnO NPs. The peaks centered at 34.58, 47.70, 56.73, 63.05, 66.51, 68.12, 69.21, and 77.12° matched with the ZnO phase, while the peaks appearing at 44.51 and 45.38 matched with the Co_3O_4 phase. It is to be noted that the peaks arising from the (100) and (101) planes of ZnO in the final composition (Co_3O_4–ZnO NCs) may also have a partial contribution from the (220) and (311) planes of the Co_3O_4 core, respectively, as it appears like a convoluted form of two peaks. Based on the diffraction peaks of Co_3O_4–ZnO NCs, the insertion of Co_3O_4 into ZnO caused a decrease in the intensity and sharpness of peaks belonging to ZnO; hence, the crystallinity of ZnO decreased. This suggests that the concentration of Co^{2+} ions has also had a marked influence on the crystalline size of the Co_3O_4–ZnO NCs.[50]

In addition, as shown in Figure 6, the number of clear diffractions and peak intensities of ZnO NPs appear to be greater than that of Co_3O_4 NPs in Co_3O_4–ZnO NCs. This suggests that ZnO NPs have a larger percentage and a high degree of crystallinity in the structure of Co_3O_4–ZnO bimetallic NCs. The reduced crystallization and intensity of the Co_3O_4 NPs peaks in the composites have been attributed to the fact that Co_3O_4 is shielded from incoming X-rays by the outer ZnO shell in the composite form, which is corroborated by prior research on the Co_3O_4–ZnO system.[61] This result suggests that the homogeneous dispersion of Co_3O_4 on ZnO crystals causes minimal lattice strain or that trace amounts of Co_3O_4 cannot be identified by an XRD device.[47] In general, the diffraction patterns of Co_3O_4–ZnO NCs show no peaks other than those of Co_3O_4 and ZnO, demonstrating that the obtained sample is impurity-free. The intensity and position of these peaks were found to be acceptable to the reference patterns Co_3O_4 (JCPDS-042-1467) and ZnO (JCPDS-36-1451), respectively, showing the successful synthesis of Co_3O_4–ZnO NCs.

The well-known Debye–Scherrer equation (eq 2) was employed for the crystalline size estimation of synthesized nanoparticles and nanocomposites.[62] Further, particle sizes were calculated from the intense peaks corresponding to the (101) plane for ZnO NPs and Co_3O_4–ZnO NCs, whereas the (220) plane for Co_3O_4 NPs was calculated using the Debye–Scherrer formula. Thus, the average crystalline sizes obtained from these peaks were 23.82, 14.79, 21.73, 16.46, and 15.99 nm for Co_3O_4 NPs, ZnO NPs, 1:4, 1:3, and 1:2 mol ratios of Co_3O_4–ZnO NCs, respectively, as shown in Table 2. The sizes and the pattern of trend (i.e., Co_3O_4 NPs > Co_3O_4–ZnO NCs > ZnO NPs) were observed for these three materials. Comparable average crystalline sizes of 16.68 nm[63] and

19.95 nm[64] were reported for Co_3O_4–ZnO NCs. The average crystalline size of the biosynthesized nanocomposites decreased as the Co_3O_4 concentration increased, according to the XRD examination. This could be because the ionic radii of the cobalt and zinc ions differ.

3.7. Scanning Electron Microscopy and Energy-Dispersive X-ray Spectroscopy (SEM-EDX) Characterization.

SEM analysis was used to determine the shape, structure, and size of the produced ZnO NPs. The SEM picture of the green-produced ZnO NPs is displayed in Figure 7a. The micrographs of ZnO NPs revealed that the particles are primarily spherical in shape and aggregate into larger particles with no well-defined morphology. Figure 7b depicts elemental composition analyses of the ZnO NPs based on the EDX plots of the SEM images. The EDX spectra revealed the excellent purity of the produced ZnO NPs. EDX measurements show three peaks ranging from 0 to 10 keV. In the tested material, those maxima are directly tied to zinc, whereas the left is related to oxygen. Other than Zn and O, no other elements were present in the sample. EDX also provides Zn and O weights and atomicity. According to the EDX results, the particles included 76.68% Zn and 23.32% O, while in the previous study, the elemental composition of zinc and oxygen was reported at 76.9% and 23.1%, respectively.[65] As indicated in Figure 7c, the average particle size of the ZnO NPs was 39.92 nm. When the SEM and EDX results are combined, they indicate that there is evidence for the formation of ZnO NPs. This observation is consistent with the presence of high-purity ZnO based on the XRD results.

Figures 8a and 9a reveal the SEM images of the 1:2 and 1:3 molar ratios of Co_3O_4:ZnO in Co_3O_4–ZnO NCs, respectively. These figures show the spherical shape and rod-shaped incorporation that may be assigned to ZnO and Co_3O_4 NPs, respectively. Figures 8b and 9b demonstrate energy-dispersive spectra (EDX) of 1:2 and 1:3 molar ratios of Co_3O_4:ZnO in Co_3O_4–ZnO NCs, respectively. The existence of Zn, Co, and O elements and their respective concentrations were assured by EDX. In addition to the expected elements, the EDX test detected Cl, which might perhaps come from the usage of the precursor $CoCl_2 \cdot 6H_2O$ even after many washings. As can be seen from the inset tables in Figures 8b and 9b, the weight percentage nearly matches the initial compositions. Hence, the preparation situations favor the successful formation of Co_3O_4–ZnO NCs successfully. Figures 8c and 9c show particle size distribution with 63.32 and 65.52 nm for 1:2 Co_3O_4–ZnO and 1:3 Co_3O_4–ZnO NCs, respectively. This result confirmed that the green synthesized composites are in the nanometer range.

3.8. Photocatalytic Activity. 3.8.1. Factors Affecting Photocatalytic Activity. 3.8.1.1. Effect of pH.

One of the most vital factors in photocatalytic processes is the pH of the solution. It has a considerable impact on the charges on the catalyst surface, which greatly influences photocatalytic activity.[66] The pH of the MG solution was changed by adding 0.1 M HCl or NaOH. To investigate the influence of pH on the photocatalytic degradation of MG dye, separate experiments were carried out at pH values ranging from 2 to 10, with a constant dye concentration (10 ppm), irradiation time (30 min), and catalyst amount (0.5 g/L), as shown in Figure 10a. The degradation of MG dye increased as the pH was increased from 2 to 8. For Co_3O_4–ZnO NCs, the percentage of elimination increases from 17.5% at pH = 2 to 90% at pH = 8. The photocatalyst degraded at a maximum rate of 90.8% in 30

Table 2. XRD Peak Positions and Average Crystalline Size of Co_3O_4, ZnO NPs and Co_3O_4 − ZnO NCs Using the Most Intense Peak

| samples	2θ (deg)	Miller indices (hkl)	fwhm (deg)	average crystalline size D (nm)
Co_3O_4 NPs	31.72	220	0.58646	23.82
ZnO NPs	36.25	101	0.68405	14.79
1:2 Co_3O_4 - ZnO	36.28	101	0.53433	15.99
1:3 Co_3O_4 - ZnO	36.39	101	0.39071	16.46
1:4 Co_3O_4 - ZnO	36.39	101	0.39071	21.73
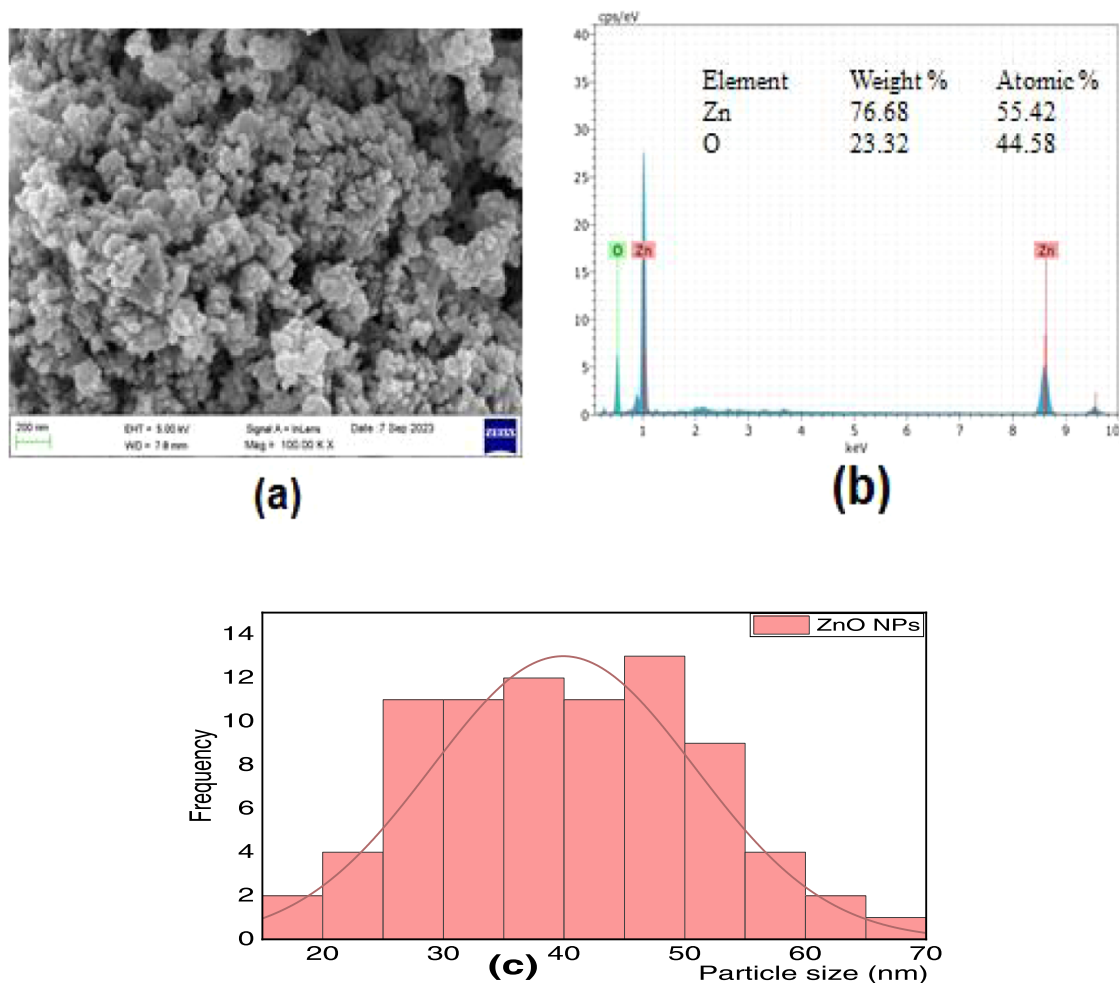
Figure 7. SEM image (a), EDX measurements (b), and particle size distribution (c) of ZnO nanoparticles.

min at a pH of 8 (Figure 10a). A rise in pH accelerates the formation of hydroxyl radicals in the reaction mixture. These hydroxyl radicals are extremely reactive in nature and can target any bond in the dye solution. As a result, at alkaline pH, the photocatalyst's number of hydroxyl groups rose, facilitating MG adsorption. The adsorption of MG onto the catalyst surface, depending on its surface area, is the most likely cause of the pH variation.[67]

3.8.1.2. Effect of Catalyst Load. Optimizing the catalyst load is a crucial aspect of reducing needless catalyst consumption. The effect of various concentrations of photocatalyst (0.1, 0.2, 0.3, 0.4, 0.5, and 0.6 g/L) at constant pH = 8, dye concentration (10 ppm), and irradiation time (30 min) was tested to determine the optimum concentration of catalyst, as shown in Figure 10b. It was found that increasing the catalyst dose from 0.1 to 0.5 g/L accelerated the degradation rate. The rise in catalytic activity with catalyst dose is due to an increase in the number of active sites present on the catalyst surface; the greater the number of active sites, the faster the formation of free radicals and therefore the accelerated degradation. However, more photocatalyst could have caused more aggregation, resulting in a decrease in the photocatalyst surface area, rendering a large fraction of the catalyst unavailable for dye adsorption. Furthermore, the degradation rate constant was reduced to an optimum value for the photocatalyst loading because the opacity of the dye solution rose and radiation was scattered, reducing the optical path. The

decline in catalytic efficiency over a certain limit is caused by turbidity in the slurry solution, which prevents light penetration through the reaction mixture and hence reduces the rate of photocatalytic activity.[68] The results showed that 0.5 g/L of catalyst was the best amount for decolorization of the dye mixture, with greater than 92.9% dye degradation accomplished after 30 min.

3.8.1.3. Effect of Dye Concentration. The effect of the initial concentration of MG on its degradation was observed by taking different initial concentrations of 10, 15, 20, and 25 ppm and fixing other parameters constant (catalyst load 0.5 g/L, pH = 8, irradiation time 30 min), as shown in Figure 10c. It was discovered that increasing the dye concentration resulted in a decrease in the rate of degradation of the dye. Excess dye concentration causes the dye to cover the active sites of the photocatalysts, reducing the path length of photons entering the solution and resulting in only a few photons reaching the catalyst surface. As a result, the generation of hydroxyl radicals is reduced. As a result, the degradation efficiency decreases.[68] It demonstrates that more molecules of dye are absorbed at the photocatalyst active sites. Furthermore, the decrease in degradation above 10 ppm may be due to decreased adsorption competition between dye molecules and OH-on the same sites, resulting in a lower rate of formation of the OH radical, which is the primary oxidant required for high degradation efficiency.[69]
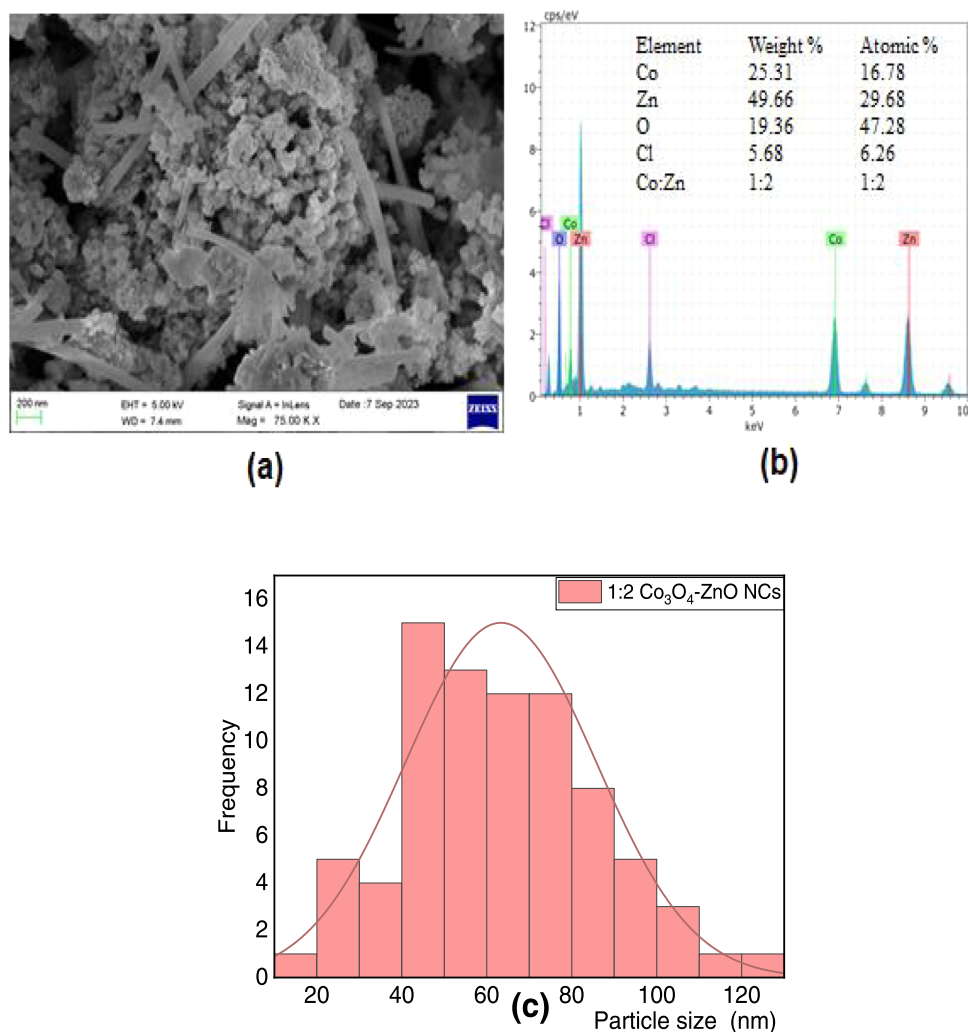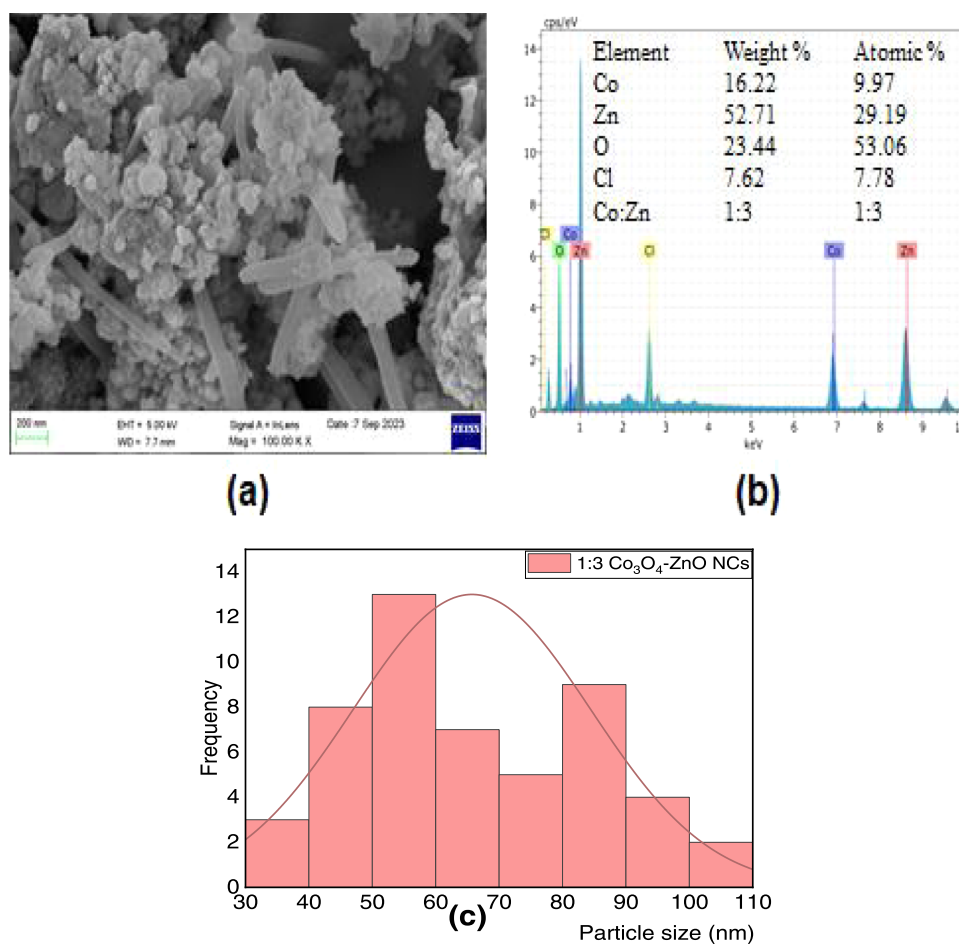
Figure 8. SEM image (a), EDX measurements (b), and particle size distribution (c) of Co_3O_4-ZnO (1:2) nanocomposites

3.8.1.4. Effect of Irradiation Time. The relationship between degradation proficiency of catalyst for MG dye degradations and irradiation time over reaction time from 0 to 60 min was examined at the optimized condition of MG at dye concentrations of (10 ppm), catalyst load (0.5 g/L), and pH of 8. The results are shown in Figure 10d. The degradation of dye by adsorption onto nanosized Co_3O_4−ZnO was shown to be slow at first but subsequently to become quick when the contact duration was increased. The dye was fully destroyed and became colorless within 60 min. After 60 min, the dye degradation achieves saturation. As a result, the optimal irradiation period for maximal elimination is determined to be 60 min. This is due to the fast adsorption rate before equilibrium; this may be explained by an increase in the number of active binding sites on the photocatalyst surface. Because there are fewer accessible sorption sites at the equilibrium stage, adsorption is most likely an attachment-controlled process.[69] The corresponding degradation proficiency of MG was found to be 90.56, 93.35, and 98.06% by 1:4, 1:3, and 1:2 Co_3O_4−ZnO NCs, respectively, as shown in Figure 10d.

3.8.2. Evaluation of Photocatalytic Activities of Green Synthesized Co_3O_4, ZnO NPs and Co_3O_4−ZnO NCs for Degradation of Malachite Green Dye. The photocatalytic activity of the synthesized Co_3O_4, ZnO NPs, and Co_3O_4−ZnO

NCs was evaluated using MG dye as a model pollutant under sunlight as a source of visible light, and the result is summarized in Figure 11a−e. With an increasing irradiation time, the absorbance spectra of the MG dye solution decreased continuously. The reduction in absorbance showed dye decolorization due to chromophore cleavage. Decreases in intensity confirm the photocatalytic degradation of the dye.

At 30 min, the intensity of all peaks in Figure 11 is slightly reduced even in the dark, which could be due to the partial adsorption of MG dye molecules on the surface of the photocatalyst. The degradation percentage was estimated using (eq 3).[69] After 40 min of radiation exposure, the dye color diminished significantly, and after 60 min of reaction, the decolorization achieved up to 98.06% for 10 ppm dye utilizing 0.5 g/LCo_3O_4−ZnO NCs. All samples show a high percentage of degradation of the MG dye, as indicated in Figure 11. Green synthesized ZnO, Co_3O_4 NPs, 1:4, 1:3, and 1:2 mol ratios of Co_3O_4−ZnO NCs revealed good photocatalytic activities with degradation efficiencies of 86.66, 88.63, 92.61, 95.98, and 98.06%, respectively, after 60 min of irradiation. Co_3O_4−ZnO NCs (1:2) showed a high percentage degradation up to 98.06%, which revealed the highly efficient activity of Co_3O_4−ZnO NCs for the degradation of MG dye. The high photoactivity of the nanocomposite could be achieved by the

Element	Weight %	Atomic %
Co	16.22	9.97
Zn	52.71	29.19
O	23.44	53.06
Cl	7.62	7.78
Co:Zn	1:3	1:3

Figure 9. SEM image (a), EDX measurements, (b) and particle size distribution (c) of Co_3O_4-ZnO (1:3) nanocomposites

presence of a synergistic effect between the components of Co_3O_4−ZnO NCs.[70]

3.8.3. Kinetics Study of the Photocatalytic Degradation of Malachite Green.

The first-order plot was fitted with this experiment, and the rate constant of MG degradation was obtained by the following equation:
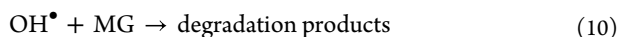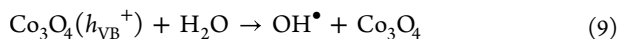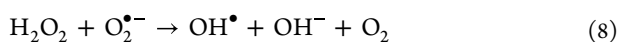
$$\ln (C_o/C_t) = kt \tag{4}$$

where t is the irradiation time, C_o is the initial concentration at time $t = 0$, C_t is the concentration at time t, and k is the apparent first-order rate constant. The linear correlation between irradiation time and $-\ln (C_t/C_o)$ indicates that the photocatalytic degradation of the MG dye shows pseudo-first-order kinetics.[71] As observed in Figure 12b, the calculated rate constants and correlation coefficients for ZnO, Co_3O_4 NPs, and various ratios of Co_3O_4−ZnO NCs are summarized in Table 3. The rate constants (k) in the degradation of MG dye with ZnO, Co_3O_4 NPs, 1:4, 1:3, and 1:2 Co_3O_4−ZnO NCs were 0.035, 0.038, 0.041, 0.053, and 0.061 min^{-1}, respectively. For the test with ZnO and Co_3O_4 photocatalysts, MG degradation under sunlight irradiation was comparatively slow. However, for Co_3O_4−ZnO heterostructures under the same experimental conditions, the reaction rate was dramatically promoted. The Co_3O_4-ZnO heterostructure showed significantly higher reaction rates due to synergism and better charge separation.[64] The adsorption reactions followed the pseudo-first-order kinetics process, demonstrating the best adsorption rate.

3.8.4. Possible Mechanism of MG Dye Degradation by Co_3O_4−ZnO Nanocomposites.

The reaction mechanism for the degradation of the MG dye by Co_3O_4−ZnO NCs was proposed as indicated in Figure 13. The degradation of MG dye by Co_3O_4−ZnO NCs is mainly due to the generation of electrons and holes (e$^-$ and h$^+$) on the catalyst surface under irradiation.[72] The p−n heterojunction between Co_3O_4 and ZnO semiconductors facilitates photogenerated electron and hole separation, leading to the formation of oxygenated free radicals and anions. These species are responsible for the formation of oxygenated free radicals and anions, which cause photocatalytic degradation of the dyes. Water molecules combine with holes and are converted into $^\bullet$OH radicals. On the other hand, the O_2 scavenges the e$^-$ and is converted into $^\bullet$OH through HOO$^\bullet$ and H_2O_2 intermediates, as shown in a series of reactions (eqs 5−10). $^\bullet$OH is a strong oxidizing species that degrades the organic molecule (dye) non-selectively into H_2O, CO_2, and inorganic ions.[73] In addition, the high surface area of the Co_3O_4−ZnO NCs synthesized in this method can be a possible reason for the effective degradation of the MG dye. Furthermore, the presence of plant extract during the synthesis of the catalysts, followed by calcinations that make the catalyst increasingly porous and improve the catalytic performances,[52] may improve photocatalytic degradation. Therefore, green synthesized Co_3O_4−ZnO photocatalysts could enhance the photocatalytic degradation activities of organic pollutants.
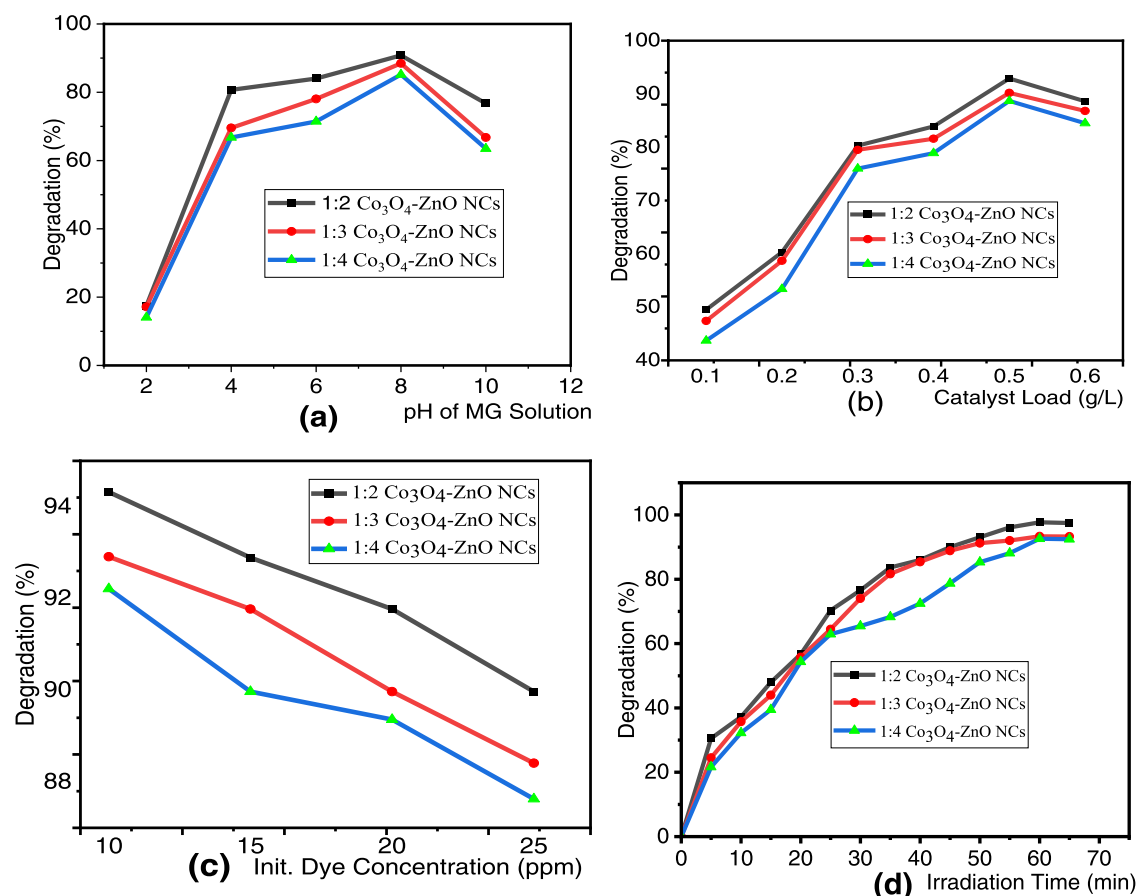
Figure 10. Optimization of (a) pH, (b) catalyst load, (c) initial dye concentration, and (d) irradiation time for MG degradation using Co_3O_4-ZnO NCs.

$$O_2 + ZnO(\overline{e}_{CB}) \rightarrow O_2^{\bullet-} \tag{5}$$

$$O_2^{\bullet-} + H_2O \rightarrow HOO^{\bullet} + OH^- \tag{6}$$

$$2HOO^{\bullet} \rightarrow H_2O_2 + O_2 \tag{7}$$

$$H_2O_2 + O_2^{\bullet-} \rightarrow OH^{\bullet} + OH^- + O_2 \tag{8}$$

$$Co_3O_4(h_{VB}{}^+) + H_2O \rightarrow OH^{\bullet} + Co_3O_4 \tag{9}$$

$$OH^{\bullet} + MG \rightarrow degradation\ products \tag{10}$$

3.8.5. Reusability of Photocatalyst (Co_3O_4-ZnO NCs). The study investigates the reusability of Co_3O_4-ZnO NCs photocatalysts for long-term heterogeneous catalysis. The catalysts were collected, washed, dried, and reused for aqueous phase degradation of MG dye under optimum conditions (pH = 8, initial concentration of MG = 10 ppm, and catalyst load = 0.5 g/L), and the results are compiled in Figure 14. The photodegradation percentages of MG for the three successive cycles of Co_3O_4-ZnO NCs were 96.13, 95.43, and 93.70%, respectively. Results showed a modest decrease in photocatalytic activity after three cycles due to the deposition of adsorbed MG molecules on the catalyst surface.[74] According to the findings, Co_3O_4-ZnO NCs are reusable photocatalysts for the degradation of MG dyes. Therefore, green synthesized Co_3O_4-ZnO photocatalysts could enhance the photocatalytic degradation activities of organic pollutants.

A brief comparison of the efficiency of MG degradation using the currently studied green synthesis of Co_3O_4-ZnO

NCs with previously reported catalysts using various methods is shown in Table 4. This comparison demonstrated how effectively the prepared materials degraded the MG dye. As indicated in Table 4, it was observed that Co_3O_4-ZnO had a higher degradation efficiency than Co^{2+}-TiO_2, La_2CuO_4-decorated ZnO, CuO-$Gd_2Ti_2O_7$, and Co_3O_4/NiO. Therefore, it is possible that the Co_3O_4-ZnO photocatalyst will work well and be acceptable to the environment in eliminating MG from contaminated (polluted) water. Since conventional methods of pollutant cleanup are ineffective and textile dyes constitute a significant class of environmental contaminants, green-produced Co_3O_4-ZnO nanocomposites offer a highly active and promising alternative for the degradation of MG dye and could potentially be used for dye treatment in textile wastewater.

3.9. Evaluation of Antibacterial Activity of Synthesized Co_3O_4, ZnO NPs, and Co_3O_4-ZnO NCs. Table 5 shows that the antibacterial properties of Co_3O_4 NPs, ZnO NPs, 1:4, 1:3, and 1:2 mol ratios of Co_3O_4-ZnO NCs at concentrations ranging from 100 to 12.5 mg mL^{-1} varied. The diffusion disk results of the antibacterial activities of the green synthesized nanoparticles and nanocomposite are given in Figure S7. Green nanoparticles and nanocomposites were found to be effective against Gram-positive (*S. aureus*) and Gram-negative (*E. coli*) bacteria. The 1:2 Co_3O_4-ZnO NCs inhibited *S. aureus* and *E. coli* growth the most, with inhibition values of 8.50 ± 0.1 and 7.5 ± 0.1 mm, respectively. Except for ZnO NPs, which had an effective concentration of 75 mg/L, the produced NPs and NCs inhibited growth at a
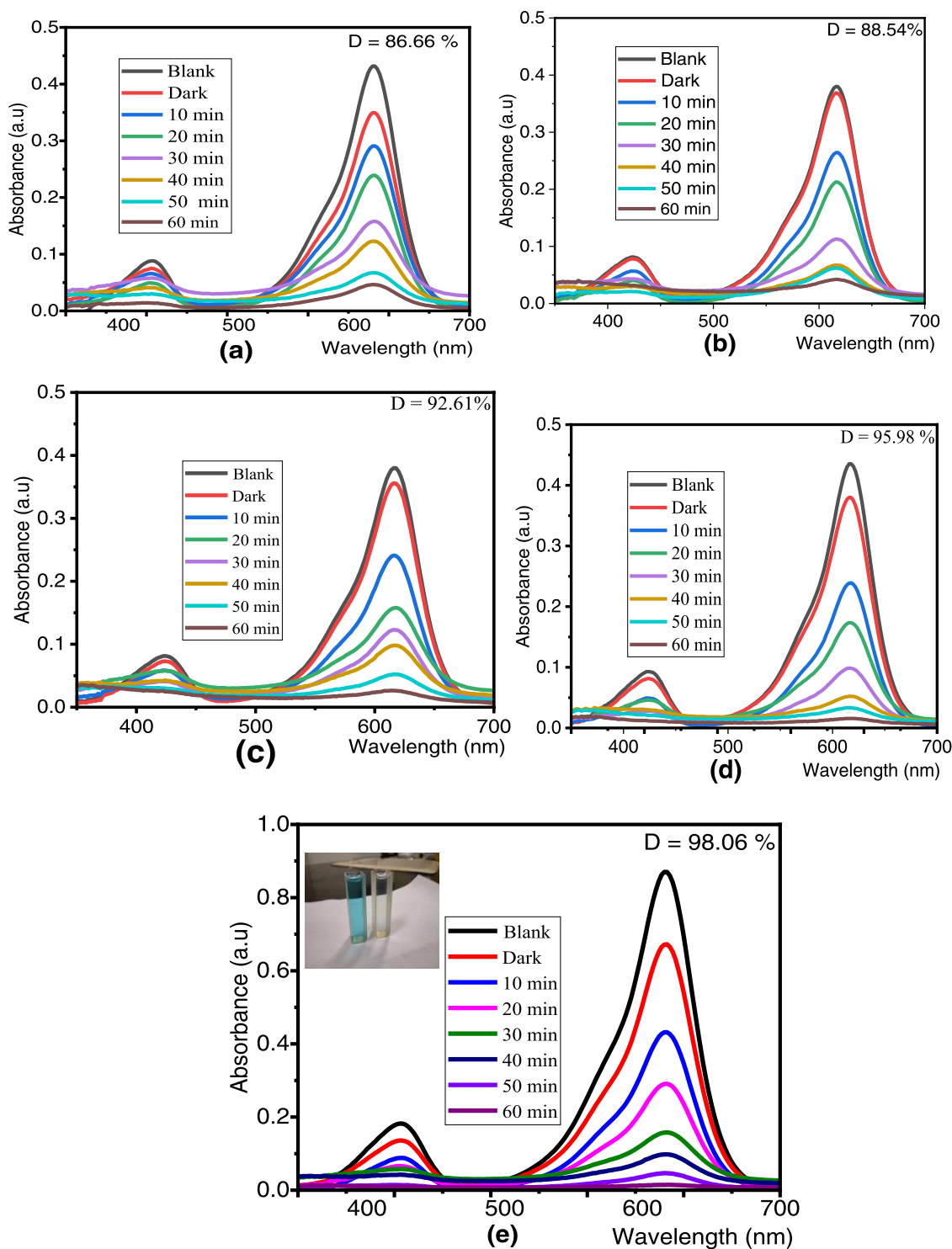
Figure 11. UV−vis spectrum of photocatalytic degradation of MG using (a) ZnO NPs, (b) Co_3O_4 NPs, (c) 1:4 Co_3O_4−ZnO NCs, (d) 1:3 Co_3O_4−ZnO NCs, and (e) 1:2 Co_3O_4−ZnO NCs.

concentration of 50 mg/L for the two strains. Bacterial growth inhibition reduces as the concentration of the NPs and NCs lowers for all samples, and there was no inhibition at 50 mg mL^{-1} for ZnO NPs and 25 mg mL^{-1} for the other samples.

Antibacterial activity was found to be more effective on *S. aureus* than on *E. coli* due to their thick cell walls and cytoplasmic membrane, which prevent certain medicines and antibiotics from entering their cells. Gram-positive bacteria also absorb nanocomposites more effectively, making them

more vulnerable to antibiotics.[80] Co_3O_4−ZnO nanocomposites inhibited Gram-positive and Gram-negative bacteria better than individual metal oxides due to more free surfaces for reactive oxygen species (ROS) generation.[81] However, paper disk diffusion bioassays did not yield good results due to the diffusion difficulties of solid NPs and NCs through agar medium.[82] Nanoparticles can cause various bactericidal and bacteriostatic effects, including improved contact with microbes, metal ion binding to DNA molecules, disruption
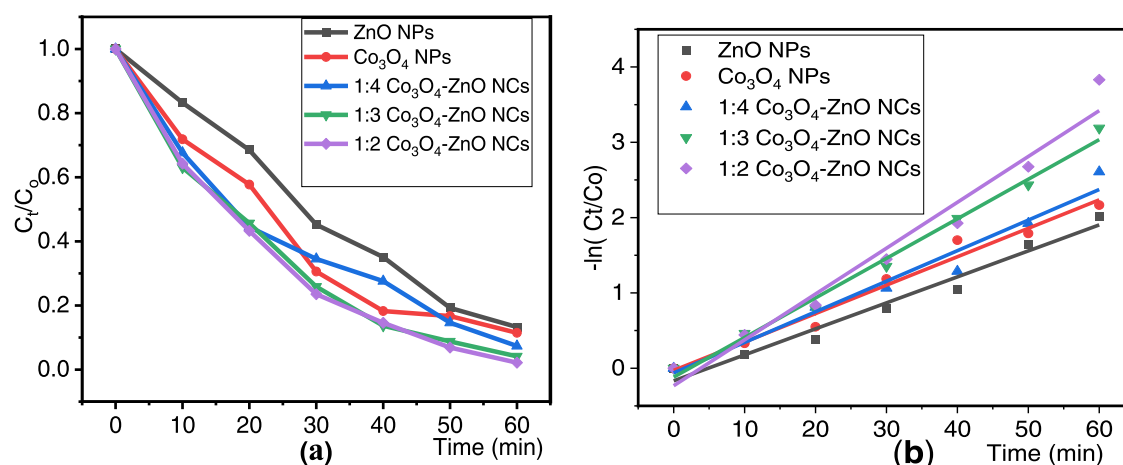
Figure 12. (a) C_t/C_o versus irradiation time plot and (b) first-order kinetic plot of MG degradation using ZnO, Co_3O_4, and various ratios of Co_3O_4-ZnO catalysts under visible light irradiation.

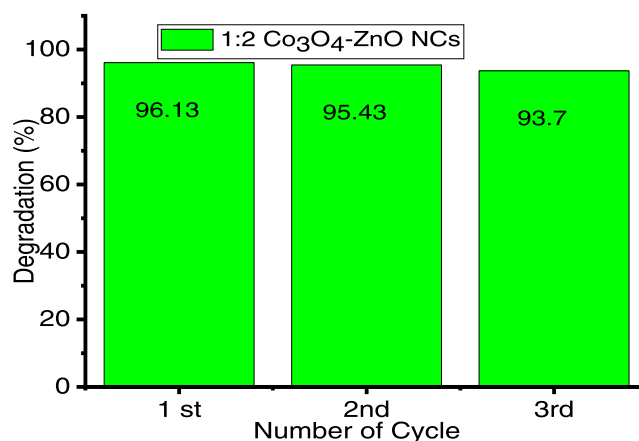**Table 3. Rate Constants and Percentage of Malachite Green Dye Degradation Using ZnO, Co_3O_4, and Co_3O_4-ZnO Catalysts under Sunlight for 60 min**

photocatalysts	linear regression coefficient (R^2)	rate constant (k) in min^{-1}	% degradation
ZnO	0.970	0.035	86.66
Co_3O_4	0.976	0.038	88.54
1:4 Co_3O_4-ZnO	0.968	0.041	92.61
1:3 Co_3O_4-ZnO	0.990	0.053	95.98
1:2 Co_3O_4-ZnO	0.966	0.061	98.06

Figure 14. Reuse of Co_3O_4-ZnO NCs for the photodegradation of MG for three successive MG cycles.

Figure 13. Proposed mechanism of photocatalytic degradation for MG dye under sunlight using the Co_3O_4-ZnO catalyst

4. CONCLUSIONS

In this study, ZnO, Co_3O_4 NPs, and Co_3O_4-ZnO NCs were synthesized via a simple and cost-effective green method using *C. aurea* leaf extract. As-synthesized samples were characterized using UV−vis, FT-IR, XRD, and SEM-EDX and evaluated for their photocatalytic and antibacterial activities. The UV−vis absorption shows peaks of ZnO at 358 nm, Co_3O_4 at 326 and 392 nm that attributed to $O^{2-} \rightarrow Co^{2+}$ and $O^{2-} \rightarrow Co^{3+}$ charge transfer processes, respectively, 1:4 Co_3O_4-ZnO NCs at 364 nm, 1:3 Co_3O_4-ZnO at 368 nm, and 1:2 Co_3O_4-ZnO at 370 nm. This significant red shift of the Co_3O_4-ZnO NCs over the pure ZnO NPs can be attributed to the presence of visible light absorptive Co_3O_4 in the Co_3O_4-ZnO NCs. FT-IR spectroscopy confirmed the nature of bonds and functional groups in leaf extract and Co_3O_4, ZnO NPs, and Co_3O_4-ZnO NCs. The results reveal peaks at 473, 560, and 658 cm^{-1}, which correspond to the stretching vibrations of Zn−O, Co^{2+}-O, and Co^{3+}−O, respectively. The purity and crystalline size of the produced materials were confirmed by the XRD patterns. The average crystalline sizes obtained from the XRD analysis were 23.82, 14.79, 15.99, 16.46, and 21.73 nm for Co_3O_4 NPs, ZnO NPs, 1:2, 1:3, and 1:4 mol ratios of Co_3O_4-ZnO NCs, respectively. The SEM results showed the spherical and rod shape and nanometer size of the synthesized materials, whereas

of metabolic processes, and the formation of reactive oxygen species (ROS). These mechanisms can lead to cell wall damage, increased membrane permeability, internalization, and the uptake of toxic metal ions.[54] Microparticles (NPs) attach themselves to bacterial cells through electrostatic interactions. Because of these interactions, bacteria experience oxidative stress due to alterations in the integrity of their cell membranes and the production of harmful free radicals. Particles with varied physical, optical, chemical, and electrical properties are produced as particle size reduces and the number of constituent atoms around the particle's surface increases, resulting in highly reactive particles (Figure 15).[4]

Table 4. Comparison of Co_3O_4−ZnO NCs Efficiencies for Degradation of MG with Previously Reported Catalysts

photocatalyst	preparation Method	light source	time (min)	percentage of degradation (%)	refs
Co_3O_4/NiO	sol−gel method	visible light	60	98	75
Co^{2+}-TiO_2	hydrothermal method	direct sunlight	120	82	76
TiO_2/Co_3O_4	green synthesis *Catharanthusroseus* (L.) G. Don leaf extract	visible light illumination	120	82.61	77
CuO-$Gd_2Ti_2O_7$	green synthesis *Acmellauliginosa* leaf extract	visible light	90	88.60	78
La_2CuO_4-decorated ZnO	green synthesis using *Strobilanthes crispus* (B.) leaf extract	visible light	120	91	79
Co_3O_4−ZnO	green synthesis using *C. aurea* leaf extract	sunlight	60	98.06	this study

Table 5. Inhibition Zone of Green Synthesized Co_3O_4, ZnO NPs, and Co_3O_4−ZnO NC against *E. coli* and *S. aureus* (Using 100 mg mL^{-1})

	antibacterial activities (zone inhibition diameter, mm)	
treatments	*E. coli* ATCC 25922	*S. aureus* ATCC 25926
Co_3O_4 NP	6.80 ± 0.1[h]	8.00 ± 0.00[d]
ZnO NP	6.50 ± 0.1[i]	7.00 ± 0.00[g]
1:2 Co_3O_4−ZnO NC	7.50 ± 0.1[e]	8.50 ± 0.1[c]
1:3 Co_3O_4−ZnO NC	7.13 ± 0.12[fg]	7.53 ± 0.06[e]
1:4 Co_3O_4−ZnO NC	6.80 ± 0.1[h]	7.30 ± 0.1[f]
erythromycin (15 μg/disk) (positive control)	19.00 ± 0.00[b]	23.00 ± 0.00[a]
DMSO (negative control)	null	null

[a]Inhibition zones (mm) designated by the different letters across rows and columns are significantly different from each other at α = 0.05 for antibacterial activities.
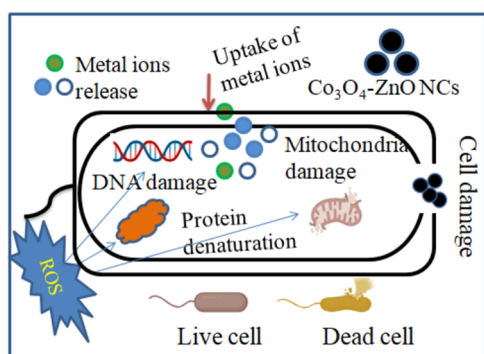
Figure 15. Proposed mechanism for antibacterial activities of Co_3O_4−ZnO nanocomposites.

EDX confirmed the presence of constituent elements of Co_3O_4−ZnO NCs. Co_3O_4−ZnO NCs showed the highest degradation efficiency, and 98.06% of the MG dye was degraded under sunlight in 60 min. In addition, the composite revealed good antibacterial activities against *S. aureus* and *E. coli*. Therefore, the *C. aurea* plant extract-mediated Co_3O_4−ZnO NC has good prospects for degradation of organic pollutants and biological applications.

ASSOCIATED CONTENT

Supporting Information

The Supporting Information is available free of charge at https://pubs.acs.org/doi/10.1021/acsomega.4c01595.

Preparation and phytochemical screening of *C. aurea* leaf extract; optimization results for reaction parameters; and flowchart of synthesis and antibacterial activity of ZnO, Co_3O_4 NPs, and Co_3O_4−ZnO NCs (PDF)

AUTHOR INFORMATION

Corresponding Authors

Kemal Mohammed Gendo − *Department of Chemistry, College of Natural and computational Sciences, Wollega University, Nekemte 395, Ethiopia;* orcid.org/0009-0003-6539-8777; Email: kemalkmg2018@gmail.com

Raji Feyisa Bogale − *Department of Chemistry, College of Natural and computational Sciences, Wollega University, Nekemte 395, Ethiopia;* orcid.org/0000-0001-6432-2736; Email: rajif@wollegauniversity.edu.et

Author

Girmaye Kenasa − *Department of Biology, College of Natural and Computational Sciences, Wollega University, Nekemte 395, Ethiopia*

Complete contact information is available at:
https://pubs.acs.org/10.1021/acsomega.4c01595

Author Contributions

Major experimental works: K.M.G.; data analysis: K.M.G., R.F.B., and GK.; methodology: KM.G, R.F.B., and G.K.; original draft writing: K.M.G., R.F.B., and G.K.; review and editing: K.M.G., R.F.B., and G.K.

Notes

The authors declare no competing financial interest.

REFERENCES

(1) Lam, S. M.; Choong, M. K.; Sin, J. C.; Zeng, H.; Huang, L.; Hua, L.; Li, H.; Jaffari, Z. H.; Cho, K. H. Construction of delaminated Ti_3C_2MXene/$NiFe_2O_4$/V_2O_5 ternary composites for expeditious pollutant degradation and bactericidal property. *J. Environ. Chem. Eng.* **2022**, *10*, No. 108284.

(2) El-Hout, S. I.; El-Sheikh, S. M.; Gaber, A.; Shawky, A.; Ahmed, A. I. Highly efficient sunlight-driven photocatalytic degradation of malachite green dye over reduced graphene oxide-supported CuS nanoparticles. *J. Alloys Compd.* **2020**, *849*, No. 156573.

(3) Saad, A. M.; Abukhadra, M. R.; Ahmed, S. A. K.; Elzanaty, A. M.; Mady, A. H.; Betiha, M. A.; Shim, J. J.; Rabie, A. M. Photocatalytic degradation of malachite green dye using chitosan supported ZnO and Ce−ZnO nano-flowers under visible light. *J. Environ. Manage.* **2020**, *258*, No. 110043.

(4) Tiki, Y. L.; Tolesa, L. D.; Tiwikrama, A. H.; Chala, T. F. Ginger (Zingiberofficinale)-Mediated Green Synthesis of Silver-Doped Tin Oxide Nanoparticles and Evaluation of Its Antimicrobial Activity. *ACS Omega* **2024**, *9* (10), 11443−11452.

(5) Nguyen, T. T. T.; Nguyen, Y. N. N.; Tran, X. T.; Nguyen, T. T. T.; Van Tran, T. Green synthesis of CuO, ZnO and CuO/ZnO nanoparticles using Annonaglabra leaf extract for antioxidant, antibacterial and photocatalytic activities. *J. Environ. Chem. Eng.* **2023**, *11*, No. 111003.

(6) Ong, C. B.; Ng, L. Y.; Mohammad, A. W. A review of ZnO nanoparticles as solar photocatalysts: Synthesis, mechanisms an applications. *Renewable Sustainable Energy Rev.* **2018**, *81*, 536−551.

(7) Sun, X.; Jiang, Z.; Li, C.; Jiang, Y.; Sun, X.; Tian, X.; et al. Facile synthesis of Co₃O₄ with different morphologies loaded on amine modified graphene and their application in supercapacitors. *J. Alloys Compd.* **2016**, *685*, 507−517.

(8) Rosen, J.; Hutchings, G. S.; Jiao, F. Synthesis, structure, and photocatalytic properties of ordered mesoporous metal-doped Co₃O₄. *J. Catal.* **2014**, *310*, 2−9.

(9) Mohammed, R.; Ali, M. E. M.; Gomaa, E.; Mohsen, M. Highly stable, reusable, and MW-assisted prepared ZnO nanorods for wastewater decontamination: Precursors ratios effect and insights on matrix and pollutants mineralization. *J. Environ. Chem. Eng.* **2021**, *9*, No. 104630.

(10) Kannan, K.; Radhika, D.; Sadasivuni, K. K.; Reddy, K. R.; Raghu, A. V. Nanostructured metal oxides and its hybrids for photocatalytic and biomedical applications. *Adv. Colloid Interface Sci.* **2020**, *281*, No. 102178.

(11) Pachaiappan, R.; Rajendran, S.; Show, P. L.; Manavalan, K.; Naushad, M. Metal/metal oxide nanocomposites for bactericidal effect: Areview. *Chemosphere* **2021**, *272*, No. 128607.

(12) Lateef, A.; Nazir, R. Metal nanocomposites: synthesis, characterization and their applications. *Sci. Appl. Tailored Nanostruct.* **2017**, 239−256.

(13) Yadav, S.; Rani, N.; Saini, K. A review on transition metal oxides based nanocomposites, their synthesis techniques, different morphologies and potential applications. *IOP Conf. Ser.: Mater. Sci. Eng.* **2022**, *1225*, No. 012004.

(14) Menon, S.; KS, S. D.; Agarwal, H.; Shanmugam, V. K. Efficacy of biogenic selenium nanoparticles from an extract of ginger towards evaluation on anti-microbial and anti-oxidant activities. *Colloid Interface Sci. Commun.* **2019**, *29*, 1−8.

(15) Chokkareddy, R.; Redhi, G. G. Green synthesis of metal nanoparticles and its reaction mechanisms. *Green Met. Nanopart.* **2018**, 113−139.

(16) Nasrollahzadeh, M.; Atarod, M.; Sajjadi, M.; Sajadi, S. M.; Issaabadi, Z. Plant-mediated green synthesis of nanostructures: mechanisms, characterization, and applications. *Interface Sci. Technol.* **2019**, *28*, 199−322.

(17) Mulata, H.; Gnanasekaran, N.; Melaku, U.; Daniel, S. Phytochemical screening and assessment of in vitro antioxidant activities of *Calpurnia aurea* seeds and leaf. *Int. J. Pharm. Pharm. Res.* **2015**, *2*, 1−12.

(18) Puttaraju, T. D.; Soundarya, T. L.; Nagaraju, G.; Lingaraju, K.; Manjula, M. V.; Devaraja, S.; Manjunatha, M. Biogenic approach for synthesis of ZnO/NiO nanocomposites as a highly efficient photocatalyst and evaluation of their biological properties. *Braz. J. Chem. Eng.* **2023**, 1−14.

(19) Bordbar, M.; Negahdar, N.; Nasrollahzadeh, M. *Melissa Officinalis* L. leaf extract assisted green synthesis of CuO/ZnO nanocomposite for the reduction of 4-nitrophenol and Rhodamine B. *Sep. Purif. Technol.* **2018**, *191*, 295−300.

(20) Kalaivani, M.; Ravi, S. Green Synthesis of ZnO NPs and CdO-ZnO Nanocomposites using aqueous Extract of Water Hyacinth (Eichhorniacrassipes) Characterization, Structural and Nano-fertilizer using Application. *Indian J. Sci. Technol.* **2023**, *16*, 1918−1926.

(21) Aragaw, S. G.; Sabir, F. K.; Andoshe, D. M.; Zelekew, O. A. Green synthesis of p-Co₃O₄/n-ZnO composite catalyst with *Eichhornia crassipes* plant extract mediated for methylene blue degradation under visible light irradiation. *Mater. Res. Express* **2020**, *7*, No. 095508.

(22) Manokari, M.; Ravindran, C. P.; Shekhawat, M. S. Biosynthesis of zinc oxide nanoparticles using Meliaazedarach L. extracts and their characterization. *Int. J. Pharm. Sci. Res.* **2016**, *1*, 31−36.

(23) Gebreslassie, H. B.; Eyasu, A. Phytochemical Screening of the Leaves *Calpurnia aurea* (Ait.)Benth Extract. *Int. J. Clin. Chem. Lab. Med.* **2019**, *5*, 18−24.

(24) Shafey, A. M. E. Green synthesis of metal and metal oxide nanoparticles from plant leaf extracts and their applications. A review. *Green Process. Synth.* **2020**, *9*, 304−339.

(25) Devatha, C. P.; Thalla, A. K. Green synthesis of nanomaterials. *Synth. Inorg. Nanomater.* **2018**, 169−184.

(26) Zhang, J.; Leng, D.; Li, G.; Liu, J.; Wang, H.; Zhu, Y.; Zhu, B.; et al. Bimetallic−organic framework-derived Co₃O₄−ZnO heterojunction nanofibers: a new kind of emerging porous nanomaterial for enhanced ethanol sensing. *Sens. Actuators, B* **2021**, *349*, No. 130732.

(27) Arab Chamjangali, M.; Bagherian, G.; Javid, A.; Boroumand, S.; Farzaneh, N. Synthesis of Ag−ZnO with multiple rods (multipods) morphology and its application in the simultaneous photo-catalytic degradation of methyl orange and methylene blue. *Spectrochim. Acta, Part A* **2015**, *150*, 230−237.

(28) Essawy, A. A. Silver imprinted zinc oxide nanoparticles: Green synthetic approach, characterization and efficient sunlight-induced photocatalytic water detoxification. *J. Cleaner Prod.* **2018**, *183*, 1011−1020.

(29) Elumalai, K.; Velmurugan, S. Green synthesis, characterization and antimicrobial activities of zinc oxide nanoparticles from the leaf extract of *Azadirachtaindica* (L.). *Appl. Surf. Sci.* **2015**, *345*, 329−336.

(30) Haq, S.; Abbasi, F.; Ali, M. B.; Hedfi, A.; Mezni, A.; Rehman, W.; Shaheen, H.; et al. Green synthesis of cobalt oxide nanoparticles and the effect of annealing temperature on their physiochemical and biological properties. *Mater. Res. Express* **2021**, *8*, No. 075009.

(31) Ezealisiji, K. M.; Siwe-Noundou, X.; Maduelosi, B.; Nwachukwu, N.; Krause, R. W. M. Green synthesis of zinc oxide nanoparticles using Solanumtorvum (L) leaf extract and evaluation of the toxicological profile of the ZnO nanoparticles−hydrogel composite in Wistar albino rats. *Int. Nano Lett.* **2019**, *9*, 99−107.

(32) TaghaviFardood, S.; Ramazani, A.; Moradi, S.; AzimzadehAsiabi, P. Green synthesis of zinc oxide nanoparticles using arabic gum and photocatalytic degradation of direct blue 129 dye under visible light. *J. Mater. Sci.: Mater. Electron.* **2017**, *28*, 13596−13601.

(33) Sunkara, J. R.; Botsa, S. M. ZnS/Fe₂O₃/Ag Ternary Nanocomposite Photocatalyst for the Degradation of Dyes Under Visible Light. *Russ. J. Phys. Chem. A* **2020**, *94*, 392−400.

(34) Merlano, A. S.; Hoyos, L. M.; Gutiérrez, G. J.; Valenzuela, M. A.; Salazar, Á. Effect ofZn precursor concentration in the synthesis of rGO/ZnO composites and theirphotocatalytic activity. *New J. Chem.* **2020**, *44*, 19858−19867.

(35) Yadav, R.; Chundawat, T. S.; Rawat, P.; Rao, G. K.; Vaya, D. Photocatalytic degradation of malachite green dye by ZnO and ZnO−β-cyclodextrin nanocomposite. *Bull. Mater. Sci.* **2021**, *44*, 1−8.

(36) Ansari, M. A.; Murali, M.; Prasad, D.; Alzohairy, M. A.; Almatroudi, A.; Alomary, M. N.; et al. Cinnamomumverum bark extract mediated green synthesis of ZnO nanoparticles and their antibacterial potentiality. *Biomolecules* **2020**, *10*, 336−350.

(37) Hashemi, S.; Asrar, Z.; Pourseyedi, S.; Nadernejad, N. Green synthesis of ZnO nanoparticles by Olive (Oleaeuropaea). *IET Nanobiotechnol.* **2016**, *10*, 400−404.

(38) Jamdagni, P.; Khatri, P.; Rana, J. S. Green synthesis of zinc oxide nanoparticles using flower extract of Nyctanthes arbor-tristis and their antifungal activity. *J. King Saud Univ., Sci.* **2018**, *30*, 168−175.

(39) Poojary, M. M.; Passamonti, P.; Adhikari, A. V. Green Synthesis of Silver and Gold Nanoparticles Using Root Bark Extract of Mammeasuriga: Characterization, Process Optimization, and Their Antibacterial Activity. *BioNanoScience* **2016**, *6*, 110−120.

(40) Rajendaran, K.; Muthuramalingam, R.; Ayyadurai, S. Green synthesis of Ag-Mo/CuO nanoparticles using Azadirachtaindica leaf extracts to study its solar photocatalytic and antimicrobial activities. *Mater. Sci. Semicond. Process.* **2019**, *91*, 230−238.

(41) Ramesh, M.; Anbuvannan, M.; Viruthagiri, G. J. Green synthesis of ZnO nanoparticles using Solanumnigrum leaf extract and their antibacterial activity. *Spectrochim. Acta, Part A* **2015**, *136*, 864−870.

(42) Senthilkumar, S. R.; Sivakumar, T. Green tea (Camellia sinensis) mediated synthesis of zinc oxide (ZnO) nanoparticles and studies on their antimicrobial activities. *Int. J. Pharm. Pharm. Sci.* **2014**, *6*, 461−465.

(43) MulyaDewi, N. O.; Yulizar, Y.; BagusApriandanu, D. O. Green synthesis of Co3O4 nanoparticles using Euphorbia heterophylla L. leaves extract: characterization and photocatalytic activity. *IOP Conf. Ser.: Mater. Sci. Eng.* **2019**, *509*, No. 012105.

(44) Huang, B.; Yang, W.; Wen, Y.; Shan, B.; Chen, R. Co3O4-modified TiO2 nanotube arrays via atomic layer deposition for improved visible-light photoelectrochemical performance. *ACS Appl. Mater. Interfaces* **2015**, *7*, 422−431.

(45) Fabbiyola, S.; Sailaja, V.; Kennedy, L. J.; Bououdina, M.; Vijaya, J. J. Optical and magnetic properties of Ni-doped ZnO nanoparticles. *J. Alloys Compd.* **2017**, *694*, 522−531.

(46) Senapati, A.; Gray, R. G.; Middleton, L. J.; Harding, J.; Hills, R. K.; Armitage, N. C. M.; PROSPER Collaborative Group. PROSPER: a randomized comparison of surgical treatments for rectal prolapse. *Colorectal Dis.* **2013**, *15*, 858−868.

(47) Alshaikh, H.; Shawky, A.; Mohamed, R. M.; Knight, J. G.; Roselin, L. S. Solution-based synthesis of Co3O4/ZnO p-n heterojunctions for rapid visible-light-driven oxidation of ciprofloxacin. *J. Mol. Liq.* **2021**, *334*, No. 116092.

(48) Urabe, A. A.; Aziz, W. J. Biosynthesis of cobalt oxide (Co3O4) nanoparticles using plant extract of Camellia sinensis (L.) Kuntze and Apiumgraveolens L. as the antibacterial application. *World News Nat. Sci.* **2019**, *24*, 357−365.

(49) Luque, P. A.; Soto-Robles, C. A.; Nava, O.; Gomez-Gutierrez, C. M.; Castro-Beltran, A.; Garrafa-Galvez, H. E.; Olivas, A. Green synthesis of zinc oxide nanoparticles using Citrus sinensis extract. *Journal of Materials Science: Materials in Electronics* **2018**, *29*, 9764−9770.

(50) Thambidurai, S.; Gowthaman, P.; Venkatachalam, M.; Suresh, S.; Kandasamy, M. Morphology dependent photovoltaic performance of zinc oxide-cobalt oxide nanoparticle/nanorod composites synthesized by simple chemical co-precipitation method. *J. Alloys Compd.* **2021**, *852*, No. 156997.

(51) Mohammadi, S. Z.; Lashkari, B.; Khosravan, A. Green synthesis of Co3O4 nanoparticles by using walnut green skin extract as a reducing agent by using response surface methodology. *Surf. Interfaces* **2021**, *23*, No. 100970.

(52) Ullah, H.; Ullah, I.; Rehman, G.; Hamayun, M.; Ali, S.; Rahman, A.; Lee, I. J. Magnesium and zinc oxide nanoparticles from datura alba improve cognitive impairment and blood brain barrier leakage. *Molecules* **2022**, *27*, 4753.

(53) Yulizar, Y.; Apriandanu, D. O. B.; Pratiwi, Y. Formation of Co3O4 nanoparticles using moringaoleifera leaves extract through two phases system of hexane-water and their photocatalytic activity. *Mater. Sci. Forum* **2020**, *982*, 9−13.

(54) Buazar, F.; Bavi, M.; Kroushawi, F.; Halvani, M.; Khaledi-Nasab, A.; Hossieni, S. A. Potato extract as reducing agent and stabiliser in a facile green one-step synthesis of ZnO nanoparticles. *J. Exp. Nanosci.* **2016**, *11*, 175−184.

(55) Yuvakkumar, R.; Suresh, J.; Saravanakumar, B.; Nathanael, A. J.; Hong, S. I.; Rajendran, V. Rambutan peels promoted biomimetic synthesis of bioinspired zinc oxide nanochains for biomedical applications. *Spectrochim. Acta, Part A* **2015**, *137*, 250−258.

(56) Chikkanna, M. M.; Neelagund, S. E.; Rajashekarappa, K. K. Green synthesis of zinc oxide nanoparticles (ZnO NPs) and their biological activity. *SN Appl. Sci.* **2019**, *1*, No. 117.

(57) Adewale Akintelu, S.; Oyebamiji, A. K.; Olugbeko, S. C.; Latona, D. F. Green chemistry approach towards the synthesis of copper nanoparticles and its potential applications as therapeutic agents and environmental control. *Curr. Res. Green Sustainable Chem.* **2021**, *4*, No. 100176.

(58) Goswami, M. Enhancement of photocatalytic activity of synthesized Cobalt doped Zinc Oxide nanoparticles under visible light irradiation. *Opt. Mater.* **2020**, *109*, No. 110400.

(59) Memon, S. A.; Hassan, D.; Buledi, J. A.; Solangi, A. R.; Memon, S. Q.; Palabiyik, I. M. Plant material protected cobalt oxide nanoparticles: sensitive electro-catalyst for tramadol detection. *Microchem. J.* **2020**, *159*, No. 105480.

(60) Okaiyeto, K.; Hoppe, H.; Okoh, A. I. Plant-based synthesis of silver nanoparticles using aqueous leaf extract of Salvia officinalis: characterization and its antiplasmodial activity. *J. Cluster Sci.* **2021**, *32*, 101−109.

(61) Jana, T. K.; Pal, A.; Chatterjee, K. Magnetic & photocatalytic study of Co3O4−ZnO nanocomposite. *J. Alloys Compd.* **2015**, *653*, 338−344.

(62) Khalil, A. T.; Ovais, M.; Ullah, I.; Ali, M.; Shinwari, Z. K.; Maaza, M. Physical properties, biological applications and biocompatibility studies on biosynthesized single phase cobalt oxide (Co3O4) nanoparticles via Sageretiathea (Osbeck.). *Arabian J. Chem.* **2020**, *13*, 606−619.

(63) Aragaw, S. G.; Sabir, F. K.; Andoshe, D. M.; Zelekew, O. A. Green synthesis of p-Co3O4/n-ZnO composite catalyst with EichhorniaCrassipes plant extract mediated for methylene blue degradation under visible light irradiation. *Mater. Res. Express* **2020**, *7*, No. 095508.

(64) Kumar, R.; Umar, A.; Kumar, R.; Chauhan, M. S.; Kumar, G.; Chauhan, S. Spindle-like Co3O4-ZnO nanocomposites scaffold for hydrazine sensing and photocatalytic degradation of rhodamine B dye. *Eng. Sci.* **2021**, *16*, 288−300.

(65) Fakhari, S.; Jamzad, M.; KabiriFard, H. Green synthesis of zinc oxide nanoparticles: a comparison. *Green Chem. Lett. Rev.* **2019**, *12*, 19−24.

(66) Samuel, M. S.; Selvarajan, E.; Mathimani, T.; Santhanam, N.; Phuong, T. N.; Brindhadevi, K.; Pugazhendhi, A. Green synthesis of cobalt-oxide nanoparticle using jumbo Muscadine (Vitisrotundifolia): Characterization and photo-catalytic activity of acid Blue-74. *J. Photochem. Photobiol., B* **2020**, *211*, No. 112011.

(67) Saleh, R.; Djaja, N. F. Transition-metal-doped ZnO nanoparticles: synthesis, characterization and photocatalytic activity under UV light. *Spectrochim. Acta, Part A* **2014**, *130*, 581−590.

(68) Siddique, M.; Khan, N. M.; Saeed, M.; Ali, S.; Shah, Z. Green synthesis of cobalt oxide nanoparticles using Citrus medica leaf extract: Characterization and photo-catalytic activity. *Z. Phys. Chem.* **2021**, *235*, 663−681.

(69) Bazazi, S.; Arsalani, N.; Khataee, A.; Tabrizi, A. G. Comparison of ball milling-hydrothermal and hydrothermal methods for synthesis of ZnO nanostructures and evaluation of their photocatalytic performance. *J. Ind. Eng. Chem.* **2018**, *62*, 265−272.

(70) Yong, Z. J.; Lam, S. M.; Sin, J. C.; Zeng, H.; Mohamed, A. R.; Jaffari, Z. H. Boosting sunlight-powered photocatalytic fuel cell with S-scheme Bi2WO6/ZnO nanorod array composite photoanode. *Inorg. Chem. Commun.* **2022**, *143*, No. 109826.

(71) Zelekew, O. A.; Kuo, D.-H.; Yassin, J. M.; Ahmed, K. E.; Abdullah, H. Synthesis of efficientsilica supported TiO2/Ag2O heterostructured catalyst with enhanced photocatalytic performance. *Appl. Surf. Sci.* **2017**, *410*, 454−463.

(72) Singh, R.; Barman, P. B.; Sharma, D. Synthesis, structural and optical properties of Ag doped ZnO nanoparticles with enhanced photocatalytic properties by photo degradation of organic dyes. *J. Mater. Sci.: Mater. Electron.* **2017**, *28* (8), 5705−5717.

(73) Lam, S. M.; Sin, J. C.; Zeng, H.; Lin, H.; Li, H.; Chai, Y. Y.; Choong, M. K.; Mohamed, A. R. Green synthesis of Fe-ZnO nanoparticles with improved sunlight photocatalytic performance for polyethylene film deterioration and bacterial inactivation. *Mater. Sci. Semicond. Process.* **2021**, *123*, No. 105574.

(74) Tran, V. A.; Phung, T. K.; Vo, T. K.; Nguyen, T. T.; Nguyen, T. A. N.; Viet, D. Q.; et al. Solar-light-driven photocatalytic degradation of methyl orange dye over Co_3O_4-ZnO nanoparticles. *Mater. Lett.* **2021**, *284*, No. 128902.

(75) Rehman, W. U.; Khattak, M. T. N.; Saeed, A.; Shaheen, K.; Shah, Z.; Hussain, S.; Bakhsh, E. M.; Alraddadi, H. M.; Fagieh, T. M.; Akhtar, K.; Khan, S. B. Co_3O_4/NiO nanocomposite as a thermocatalytic and photocatalytic material for the degradation of malachite green dye. *J. Mater. Sci.: Mater. Electron.* **2023**, *34*, No. 15.

(76) Kamble, R. J.; Gaikwad, P. V.; Garadkar, K. M.; Sabale, S. R.; Puri, V. R.; Mahajan, S. S. Photocatalytic degradation of malachite green using hydrothermally synthesized cobalt-doped TiO2 nanoparticles. *J. Iran. Chem. Soc.* **2022**, *19*, 303−312.

(77) Syahfitri, T. W. W.; Yulizar, Y.; Gunlazuardi, J.; Apriandanu, D. O. B. TiO_2/Co_3O_4 nanocomposite: Synthesis via Catharanthusroseus (L.) G. Don leaf extract, characterization and its photocatalytic activity for malachite green degradation. *IOP Conf. Ser.: Mater. Sci. Eng.* **2020**, *902*, No. 012003.

(78) Halomoan, I.; Yulizar, Y.; Surya, R. M.; Apriandanu, D. O. B. Facile preparation of CuO-$Gd_2Ti_2O_7$ using Acmellauliginosa leaf extract for photocatalytic degradation of malachite green. *Mater. Res. Bull.* **2022**, *150*, No. 111726.

(79) Yulizar, Y.; Apriandanu, D. O. B.; Ashna, R. I. La_2CuO_4-decorated ZnO nanoparticles with improved photocatalytic activity for malachite green degradation. *Chem. Phys. Lett.* **2020**, *755*, No. 137749.

(80) Naseer, M.; Aslam, U.; Khalid, B.; Chen, B. Green route to synthesize Zinc Oxide Nanoparticles using leaf extracts of Cassia fistula and *Meliaazadarach* and their antibacterial potential. *Sci. Rep.* **2020**, *10*, No. 9055.

(81) Jan, T.; Azmat, S.; Mansoor, Q.; Waqas, H. M.; Adil, M.; Ilyas, S. Z.; Ahmad, I.; Ismail, M. Superior antibacterial activity of ZnO-CuO nanocomposite synthesized by a chemical Co-precipitation approach. *Microb. Pathog.* **2019**, *134*, No. 103579.

(82) Bhuyan, T.; Mishra, K.; Khanuja, M.; Prasad, R.; Varma, A. Biosynthesis of zinc oxide nanoparticles from Azadirachtaindica for antibacterial and photocatalytic applications. *Mater. Sci. Semicond. Process.* **2015**, *32*, 55−61.